Journal of Building Engineering 96 (2024) 110474

Contents lists available at ScienceDirect

Journal of Building Engineering

journal homepage: www.elsevier.com/locate/jobe

Displacement ventilation: A systematic review of the interactions with indoor environment and simplified modelling approaches

Giacomo Tognon *, Angelo Zarrella

Department of Industrial Engineering - Applied Physics Section, University of Padova, Via Venezia 1, 35131, Italy

ARTICLE INFO

Keywords:
Displacement ventilation
Temperature distribution
Airflow field
Indoor air quality
Energy performance
Modelling

ABSTRACT

Displacement ventilation is a buoyancy-driven air distribution strategy exploiting the convective heat sources' thermal plumes to push the contaminants towards the ceiling. This review paper first analyses several aspects of the interaction between the displacement ventilation system and the enclosed space. In particular, the aspect of characteristic thermal stratification and air quality inside the thermal environment are presented. Then, the energy performance of displacement ventilation system is analysed. Secondly, the simplified modelling approaches to consider the displacement ventilation in building energy simulations are presented, examining their strong and weak points. To this purpose, the use of analytical models and empirical formulations are investigated. Also, nodal and zonal models for prediction of the vertical temperature profile are taken into account. Simplified cooling load calculation methods are also proposed to study the system energy performance while still using the well-mixed building models.

Nomenclature

List of symbols

A	Surface/opening area	[m^2]
A^*	Effective opening area	[m^2]
Ar	Archimedes number	[−]
B	Buoyancy flux	[$m^4\ s^{-3}$]
C	Concentration	[ppm]
C_d	Discharge coefficient	[−]
C_e	Flow contraction coefficient	[−]
C_{pl}	Plume constant	[$s\ m^{-3}$]
c_p	Specific heat	[$J\ kg^{-1}\ K^{-1}$]
g	Gravitational acceleration	[$m\ s^{-2}$]
H	Room height	[m]
h	Height	[m]
N	Number of points (measuring points/CFD cells)	[−]
Q	Volumetric flow rate	[$m^3\ s^{-1}$]
q	Heat load	[W]
T	Temperature	[°C]
t	Time	[s]
v	Velocity	[$m\ s^{-1}$]

(*continued on next page*)

* Corresponding author.
E-mail address: giacomo.tognon.2@studenti.unipd.it (G. Tognon).

https://doi.org/10.1016/j.jobe.2024.110474
Received 22 May 2024; Received in revised form 12 August 2024; Accepted 14 August 2024
Available online 15 August 2024

(*continued*)

List of symbols		
W	Heat source generation	[W]
α	Entrainment coefficient	[−]
α_c	Convective heat transfer coefficient	[W m^{-2} K^{-1}]
α_r	Radiative heat transfer coefficient	[W m^{-2} K^{-1}]
β	Volumetric expansion coefficient	[K^{-1}]
γ	Heat gain contribution to the occupied zone's thermal balance	[−]
ΔT	Temperature difference	[°C]
ε_a	Air Change Efficiency	[−]
ε_c	Contaminant Removal Effectiveness	[−]
ε_{exp}	Personal exposure index	[−]
ε_t	Heat Removal Effectiveness	[−]
θ	Dimensionless temperature	[−]
ρ	Density	[kg m^{-3}]
τ	Age of air	[s]
τ_n	Room nominal time constant	[s]

Subscripts	
0.1m	At a height of 0.1 m from the floor
1.1m	At a height of 1.1 m from the floor
1.7m	At a height of 1.7 m from the floor
a	Air
af	Air layer above the floor
avg	Average
b	Bottom opening
bz	Breathing zone
c	Convective
coil	Cooling coil
cond	Conductive
entr	Entrainment
ex	Heat transmission through external building structures
exh	Exhaust
exh-sup	Difference between exhaust and supply
exhal	Exhaled
exp	Exposure
f	Floor
gains	Internal heat gains
head-feet	Difference between head and feet levels
inh	Inhaled
l	Overhead lighting
loc	Local
norm	Normalized
occupied	Occupied zone
oe	Heat sources in the occupied zone
out	Outdoor air
oz	Occupied zone
p	At a given point in the room
plume	Thermal plume
r	Radiative
set	Setpoint
space	Whole space
ss	Steady-state
supply	Supply
sur	Surface
t	Top opening
tot	Total load
vent	Ventilation load
well-mixed	Ideal well-mixed case
zone	Target zone

Acronyms		
AAHS	Average Accessibility of the Heat Source	[−]
ACE	Air Change Efficiency	[−]
ACH	Air Changes per Hour	[h^{-1}]
ADPI	Air Diffusion Performance Index	[%]
AHU	Air Handling Unit	
AIIR	Airborne Infection Isolation Room	
ASHRAE	American Society of Heating, Refrigerating and Air-Conditioning Engineers	
BES	Building Energy Simulation	

(*continued on next page*)

(*continued*)

List of symbols		
CAV	Constant Air Volume	
CBL	Convective Boundary Layer	
CC	Cooling Ceiling	
CF	Cooling Floor	
CFD	Computational Fluid Dynamics	
COVID-19	COronaVIrus Disease 19	
CRE	Contaminant Removal Effectiveness	[−]
CRI	Contribution Ratio of Indoor climate	[−]
CW	Cooling Wall	
DR	Draft Rate	[%]
DV	Displacement Ventilation	
ECLF	Effective Cooling Load Factor	[−]
EDT	Effective Draught Temperature	[°C]
ERAT	Equivalent Room Air Temperature	[°C]
ESAR	Equivalent Supply Airflow Rate	[h^{-1}]
ESAT	Equivalent Supply Air Temperature	[°C]
FFD	Fast Fluid Dynamics	
HC	Heating Ceiling	
HF	Heating Floor	
HFC	Heating Floor and Ceiling	
HRE	Heat Removal Effectiveness	[−]
HVAC	Heating Ventilation and Air Conditioning	
IAQ	Indoor Air Quality	
IF	Intake Fraction	[−]
LCL	Local Cooling Load	[W]
LES	Large Eddy Simulation	
MAA	Mean Age of Air	[s]
MV	Mixing Ventilation	
PCB	Passive Chilled Beams	
PMV	Predicted Mean Vote	[−]
PD	Percentage Dissatisfied	[%]
PPD	Predicted Percentage Dissatisfied	[%]
RANS	Reynolds-Averaged Navier-Stokes	
REHVA	Representatives of European Heating and Ventilation Associations	
SGS	Sub-Grid Scale	
STRAD	STRatified Air Distribution	
SV	Stratum Ventilation	
TRNSYS	TRaNsient SYStem simulation program	
VAV	Variable Air Volume	
VOC	Volatile Organic Compound	

1. Introduction

Currently, the building sector is responsible for 40 % of overall energy consumption and 36 % of greenhouse gas emissions in Europe [1]. The European Commission has established that the existing building stock must be renovated to reach complete decarbonisation within 2050 [2]. Building energy use is mainly related to the operation of the HVAC plant, which plays a fundamental role in ensuring adequate indoor comfort levels. Indeed, occupants' satisfaction towards the indoor environment is strongly related to their well-being and productivity [3].

Reducing building-related energy costs is challenging and can be fostered by improving the efficiency of single components or the entire system and lowering the heating and cooling loads. Besides the adequate thermal insulation of the envelope, airtightness is another characteristic sought in new buildings [4]. Minimising the adventitious air inflows through the envelope gaps from the outdoors involves a decrease in the infiltration load to be offset for air conditioning. However, this measure implies the necessity of a well-designed ventilation system for maintaining suitable levels of indoor air quality (IAQ). The purpose is to replace the indoor stale air with fresh air from the external environment, and it can be achieved through different strategies: natural, mechanical and hybrid ventilation [5].

According to the airflow and thermal field, the ventilation methods can be subdivided into two categories, i.e., fully mixed and non-uniform. Recently, unsteady air distribution systems producing fluctuations in indoor parameters and airflow over time (e.g., intermittent and pulsating ventilation) have also been studied, proving their effectiveness in thermal comfort, indoor air quality and virus spread control [6–8]. Traditional mixing ventilation (MV) systems apply the perfect mixing approach, seeking uniformity in the indoor environment. On the other hand, non-uniform ventilation strategies aim to ventilate a reduced portion of the entire space; thus, the system has to offset a lower thermal load compared to conventional mixing, whose target is heating/cooling the whole room volume. Regarding the healthiness of the space related to the quality of the indoor air, the mixing air distribution strategy pursues the dilution of indoor pollutants, leading to a uniform contaminant concentration over the room volume, whereas non-uniform methods aim at removing the contaminants by displacing them towards the unoccupied zone and preventing its spread in points far from the emitting sources.

Non-uniform distribution strategies can be subdivided into piston type (e.g., piston ventilation), stratified (e.g., underfloor air distribution, displacement ventilation) and task zone (e.g., personalised ventilation) ventilation systems [9,10]. The stratified air distribution (STRAD) systems are conceived to push the contaminants emitted from occupants or other sources towards the upper part of the room and exhaust them by installing outlet grilles near the ceiling. Their main characteristic is the vertical thermal stratification they generate in the ventilated environment, which could be troublesome for thermal comfort perceived by occupants if unacceptable temperature gradients are reached [11–14]. From this point of view, the design process of such air distribution systems is challenging.

Among stratified ventilation techniques, displacement ventilation (DV) is a recognized and consolidated system [15]. Initially introduced in Scandinavian countries to improve air quality and energy efficiency in industrial premises, its application rapidly broadened, involving non-industrial facilities, such as offices, schools, and other commercial buildings. Fig. 1 shows the operating principle of a conventional DV system [16]. The inlet and outlet vents are placed at floor and ceiling levels, respectively. The supply air directly enters the occupied zone through low-site diffusers at low velocity and an inlet temperature slightly below the target room temperature. The cooler fresh air spreads over the floor, heats up when encountering the heat sources and rises towards the ceiling. The upward flow in the convective boundary layer (CBL) around the heat source surface and the thermal plume above it bring the contaminants into the upper part of the room, where they accumulate and are extracted. This ventilation concept produces stratification of the indoor environment in temperature and contaminant distribution; ideally, the space is roughly subdivided into a lower cleaner layer, corresponding to the occupied zone, and an upper polluted layer near the ceiling. The effectiveness of displacement ventilation is based on adequately exploiting the buoyancy effect driven by the heat sources. Its design phase is rather challenging, for which schematic guidelines can be found in the literature [17], and detailed guidebooks are provided by international associations, e.g., ASHRAE [18] and REHVA [16].

The outbreak of the COVID-19 pandemic has roused a specific interest in building ventilation concerning its design and management [19,20]. It is well-known that there is a positive correlation between ventilation and a decrease in health issues related to life in buildings, such as airborne respiratory diseases, although there are no universally applicable rules on the minimum outdoor airflow rates required to avoid health risks in all public and residential buildings [21]. By now, it is ascertained that the coronavirus can infect people through different modes: by contact (direct or indirect), by large exhaled droplets landing on susceptible subject's bare body parts, and by airborne transmission caused by infectious microdroplets (called *droplet nuclei*) remaining suspended in the indoor air and transported following airflow patterns [22,23]. For this reason, the ventilation of indoor spaces providing an adequate amount of outdoor air is strongly recommended as an effective mitigation strategy against the airborne infection risk [24]. In this panorama, displacement ventilation has drawn renewed attention: its use is preferable to a traditional mixing system since it physically removes pathogens from the occupied space rather than spreading them all over the room, as a dilution process would do [25,26].

This paper reviews the scientific literature to analyse the state-of-the-art research on displacement ventilation. This air distribution strategy is examined from two perspectives. Firstly, the characteristics and the interaction between DV and the ventilated environment are investigated. In this context, different aspects related to DV operation are addressed: the resulting temperature field and the corresponding level of thermal comfort achieved, the airflow distribution, indoor air quality and ventilation effectiveness, and energy use. The main research techniques adopted to understand the environment behaviour under DV operation are also presented. Despite thermal comfort and IAQ being essential aspects to analyse during the operation of ventilation systems, the evaluation of their performance in terms of energy costs must be considered, and its impact on the overall energy demand cannot be neglected. Therefore, the second part presents and discusses the development of simplified models for displacement ventilation. DV involves a complex fluid dynamic phenomenon, thus, the search for simple tools to simulate the air distribution patterns and the thermal environment is fundamental, as they can be integrated into typical building energy simulations without resorting to detailed modelling methods, e.g.,

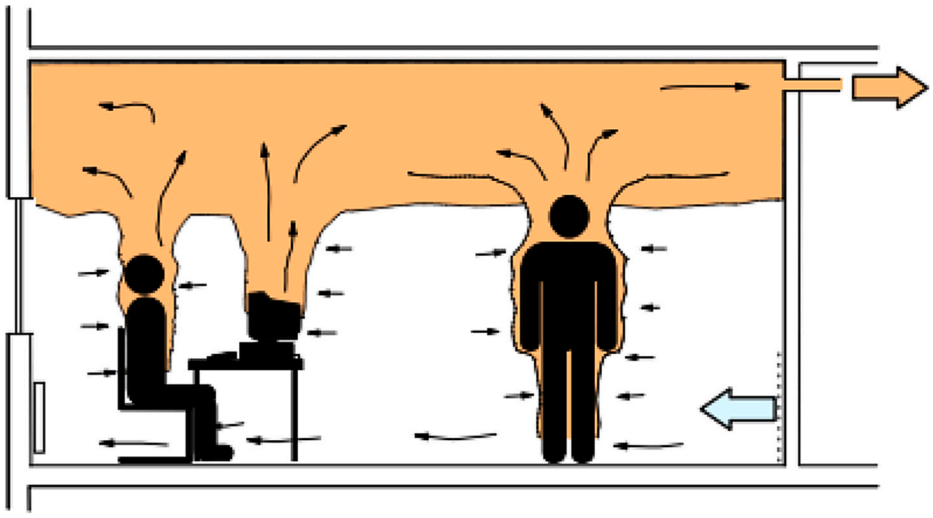

Fig. 1. Displacement ventilation concept (taken from Ref. [16]).

CFD analysis (computational fluid dynamics). To the best of the authors' knowledge, the only existing review dealing exclusively with displacement ventilation [15] is dated, so this work is proposed to highlight the results from more recent research activities, illustrating if the current direction the research field on the topic has taken is different from older studies or if the baseline is the same. Moreover, Yuan's review [15] and guidebooks [16,18] mainly focus on the design phase of DV systems by proposing step-by-step procedures. However, the expanding use of building energy simulation (BES) tools requires appropriate and computationally efficient DV modelling approaches. Generally, the perfect mixing approach is employed in the multi-zone simulations, but reliable results cannot be obtained if the analysed buildings adopt displacement ventilation. In this context, no previous work dealt with this aspect; therefore, this paper provides a detailed overview of the simplified modelling strategies for simulating DV performance currently available in the scientific literature that have not yet been critically collected. It could help engineers in the design phases, analyse the energy performance of DV systems, outline their optimal operation management or suggest potential retrofit solutions regarding ventilation strategies.

2. Methodology and materials

The present review was developed upon a consistent selection of relevant papers out of more than 180 found in the literature. The starting point regards the reasons that have driven the activity, in particular, looking at the aspects characterising the research on DV in a comprehensive way. The review tries to answer to the following main opening questions:

- How does DV work and what are its driving forces?
- What are the main characteristics of displacement ventilated environments regarding temperature, airflow, and contaminant distribution over air volume?
- What are the advantages of the DV system compared to other air distribution strategies, especially the conventional widespread MV systems?
- Are there simplified models properly describing DV systems and their behaviour that could support building simulation tools in carrying out reliable energy analyses?

After formulating the review objectives, the search for original research articles has been conducted primarily through Science Direct [27] and Web of Science [28] databases. Moreover, guidebooks and documents published by the most important organisations dealing with energy in buildings and HVAC systems (e.g., ASHRAE in the U.S. and REHVA in Europe) have been included. Although the analysed period goes from 1990 to 2022, most of the material included belongs to the last decade to highlight the current research focus.

The workflow with the search process phases is schematically shown in Fig. 2. Specific terms have been employed for the research, such as "thermal comfort", "temperature distribution", "stratification", "indoor air quality", "contaminant distribution", "ventilation effectiveness", "COVID-19", "airborne transmission", "infection risk", "energy", "energy performance", "energy efficiency", "model", "simplified model", "nodal model", all combined with the paramount keyword "displacement ventilation". At first, the papers were

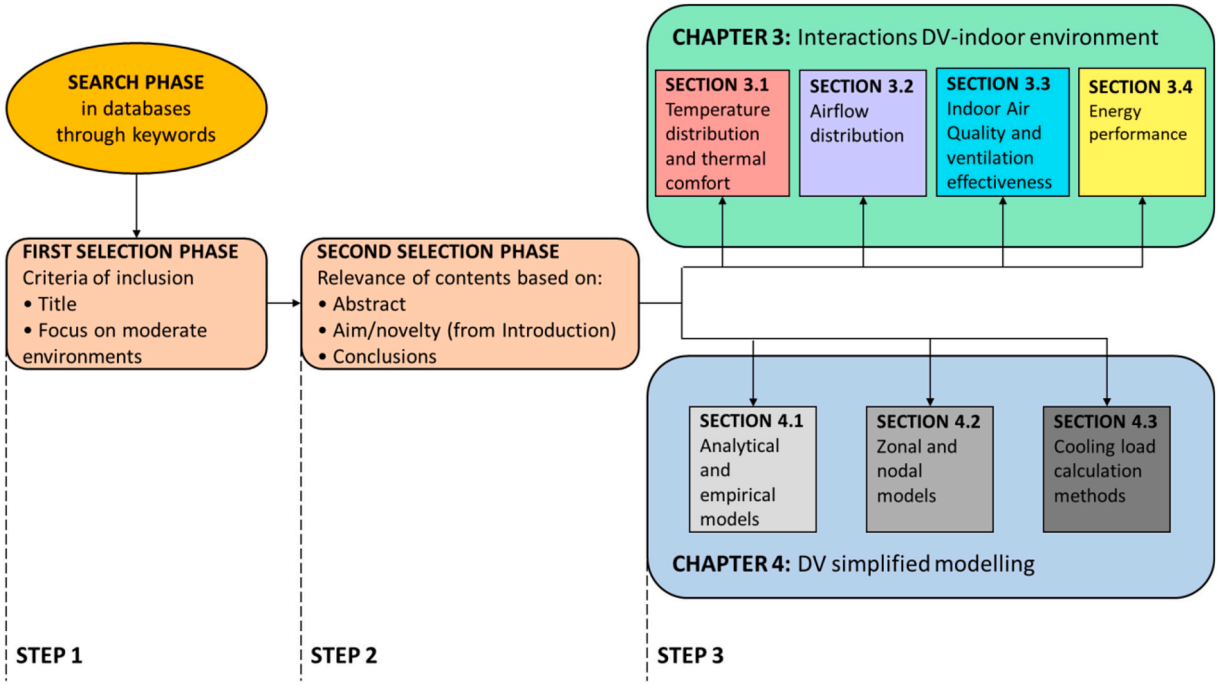

Fig. 2. Workflow of the search and selection phases of the literature material.

chosen based on title and only if dealing with moderate environments (i.e., offices, school classrooms, commercial and residential buildings in general), whereas industrial or severe environments are not part of the paper. In the second step, the most significant papers were extracted according to the abstract's contents, the study's objective, and the conclusions; those selected were analysed in more detail, and the most interesting results were drawn. Based on the subject of investigation, each paper has been associated with a specific category corresponding to the successive sections of the review.

Both natural and mechanical systems are included in the analysis to give a complete overview of the DV operation. The working principle is essentially the same, as the internal heat sources drive the upward airflows in the form of thermal plumes. In the case of natural DV, the stack effect generated by the buoyant sources produces the air movement, which acquires the form of a rising displacement flow if a floor-level and a ceiling-level vent are installed, becoming the inlet and outlet of the system, respectively. On the other hand, outdoor air is supplied through fans in a mechanical DV system, and the momentum of the inlet air jet contributes to the flow equilibrium in combination with the buoyancy forces.

3. Interaction with the enclosed space

The interaction between the displacement ventilation system and indoor space produces a characteristic environment. As shown in Fig. 1, supply air flows along the floor at low temperature and velocity, heats up encountering the heat source and rises bringing contaminants towards the ceiling and generating thermal stratification. The research activities are oriented to investigate one or more features of DV, which can be divided into four categories: temperature distribution, airflow distribution, indoor air quality, and energy consumption. A suitable assessment of the behaviour of displacement ventilation rooms requires that environmental parameters are known with a certain level of detail within the fluid dynamic field; hence, the more frequently adopted investigation approaches are experimental testing and detailed numerical modelling through CFD analysis [29]. Experimental methods can be further distinguished between the salt bath technique and measurement campaigns. The former is widely employed to study buoyancy and convection flows [30]. In salt-bath systems, water is used as a surrogate of air to simulate the displacement flow. Small parallelepiped-shaped tanks represent reduced scaled models of real building rooms, and they are placed inside a larger reservoir containing the working fluid, which stands for the external environment surrounding the building. Typically, these tests are conceived to study natural DV driven by density differences between indoor and outdoor environments or buoyant sources if appropriately positioned inlet and outlet enable the flow regime development. Water is usually the lighter fluid, whereas a brine (water with a certain salt concentration) simulates the denser fluid. Flow visualization techniques can be employed when dyeing one fluid to detect the dynamic flow distribution and the formation of steady-state stratification if a continuous buoyancy source is present. Most researchers adopt a reverse flow orientation compared to real building ventilation: water is the ambient fluid (lighter), while the plume source supplies the brine (denser), inducing an inflow from the upper openings and an outflow at the bottom. However, the experimental set-up can also be arranged to resemble the DV flow occurring in a real building, with brine as ambient external fluid and fresh water injected as the buoyant plume [31].

Though salt-bath experiments are useful to reveal the density stratification of the space, water properties are different from those of air, affecting both mass and heat transfers in the system equilibrium. On the other hand, the direct measurement of environmental parameters in displacement ventilated spaces gives the most indicative information on the actual behaviour of the ventilated room. Experimental tests can regard both laboratory setups and field measurements. In the first case, climatic chambers under controlled conditions are used. The possibility of setting and modifying the boundary conditions is favourable as different system configurations can be tested one after the other. On the other hand, on-site measurement campaigns provide a real representation of the actual buildings' behaviour under DV. Indeed, boundary conditions are time-variant, and external disturbances cannot be controlled as precisely as in laboratory facilities. In both cases, air temperatures and velocities are measured to describe the fluid dynamic domain, whereas CO_2 or other tracer gas concentrations are used as markers of indoor air quality. Since temperature and contaminant stratification occur with DV, sensors must be put at different heights to observe this aspect.

The larger the number and the higher the spatial resolution of measuring points, the greater detail of information about the thermal environment is obtained; nevertheless, this would imply higher costs for instrument procurement and installation. Another weak point of the experimental approach is that the geometrical size of the tested room is fixed, just as the ventilation system layout cannot usually be changed; thus, different configurations can rarely be proposed. To overcome these issues, many researchers choose a numerical simulation approach. Displacement ventilation flow can be effectively represented through CFD modelling. In CFD analyses, the Navier-Stokes equations expressing mass, energy conservation and momentum balance are numerically solved to define the fluid dynamic field. Since a fine discretisation grid (*mesh*) is applied to the domain, the environmental parameters are calculated with a high spatial resolution, reaching a high degree of detail. This approach is apt to simulate systems with different layouts and boundary conditions. However, CFD models present some drawbacks, as well. Firstly, they need to be validated through measured data before being used for other case studies. More importantly, the computational costs required for running a simulation are significant depending on the desired level of detail and problem size. Gilani et al. investigated the performance of steady Reynolds-averaged Navier-Stokes (RANS) CFD in predicting temperature and age of air distributions in a space with a heat source driving a displacement flow, conducting a sensitivity analysis to evaluate the influence of the modelling settings, i.e., computational grid resolution, turbulence model, discretisation scheme and iterative convergence criterion. They concluded that the accuracy and reliability of CFD estimations can be improved by implementing k-ω turbulence models and setting smaller residuals for convergence, respectively [32]. Similarly, Taghinia et al. tried to describe the airflow pattern, temperature and velocity distribution around the human body, adopting large eddy simulation (LES) and hybrid LES-RANS methods. The sub-grid scale (SGS) model used to represent small-scale turbulent motions affects the accuracy of predictions, especially in the region close to the human body surface [33]. Jin et al. employed coarse-grid fast fluid dynamics (FFD) to simulate buoyancy-driven displacement flow. The estimation of thermal stratification presents

accuracy similar to fine-grid FFD simulations at a much lower computational time if a thermal plume model is integrated into momentum and energy equations for capturing the plume flow in the cells influenced by the heat sources [34].

3.1. Thermal environment

Displacement ventilation is essentially driven by buoyancy forces. The supply air directly enters the room through floor-level diffusers at an inlet temperature slightly lower than the average desired temperature in the occupied space. It heats up coming into contact with internal gains and rises in the form of upward convective flows or thermal plumes, exploiting the density differences. The outcome is a stratified flow in the ventilated space, which presents a vertical temperature gradient between supply and exhaust. This vertical variation can be described in terms of dimensionless temperature, expressed in Eq. (1).

$$\theta = \frac{T - T_{supply}}{T_{exh} - T_{supply}} \tag{1}$$

Where T, T_{supply} and T_{exh} are the air temperature at a given height, at the supply and the exhaust, respectively.

Due to non-uniformity in the space temperature field, potential conditions of thermal discomfort may arise for occupants. The level of thermal comfort achieved in a stratified environment can be described following the classical comfort model based on PMV/PPD indexes [13,14], for which a distribution is obtained rather than a single value, in contrast to well-mixed enclosures. In particular, the characteristic stratification may cause discomfort if a large vertical temperature gradient is produced within the occupied zone. The vertical air temperature difference is calculated between head and ankle levels through Eqs. (2) and (3) for seated and standing people, respectively.

$$\Delta T_{a,1.1m} = T_{a,1.1m} - T_{a,0.1m} \tag{2}$$

$$\Delta T_{a,1.7m} = T_{a,1.7m} - T_{a,0.1m} \tag{3}$$

Where T_a denotes the air temperature. The ankle level is 0.1 m above the floor, whereas the head level is 1.1 m or 1.7 m for a sitting and a standing person, respectively. Current standards propose a maximum vertical air temperature difference of 3 °C for a seated person [13,14] and 4 °C for a standing occupant [13] to keep the percentage of dissatisfied people (PD) below 5 %. Although DV can preserve comfort conditions, with PMV distribution ranging from −0.5 and 0.5 and PPD below 10 % [35], adequate operating conditions, i.e., supply temperature and flow rate, must be set to avoid temperature gradient issues [36,37].

Two zones are typically identified under DV operation: a lower zone where an upward airflow motion and a progressive stratification exist with an almost linear temperature distribution and an upper layer where recirculation occurs, producing a mixing effect and thermal uniformity. The stratification or mixing layer height is the two layers' intermediate interface. Fig. 3 schematically illustrates the phenomenon with the presence of an occupant as a heat source; the flow patterns and the approximate temperature distribution are highlighted.

The development of the overall temperature gradient and the separating layer location strongly depend on the interaction between ventilation and internal heat gains. The heat source produces a rising thermal plume, which increases its volume flow rate entraining the surrounding air [38] and the interface layer forms where it matches the supply flow rate from the ventilation system. The DV steady operation is driven by the balance between buoyancy and supply momentum, whose ratio is defined by the dimensionless Archimedes number, expressed in Eq. (4) (from Ref. [39]).

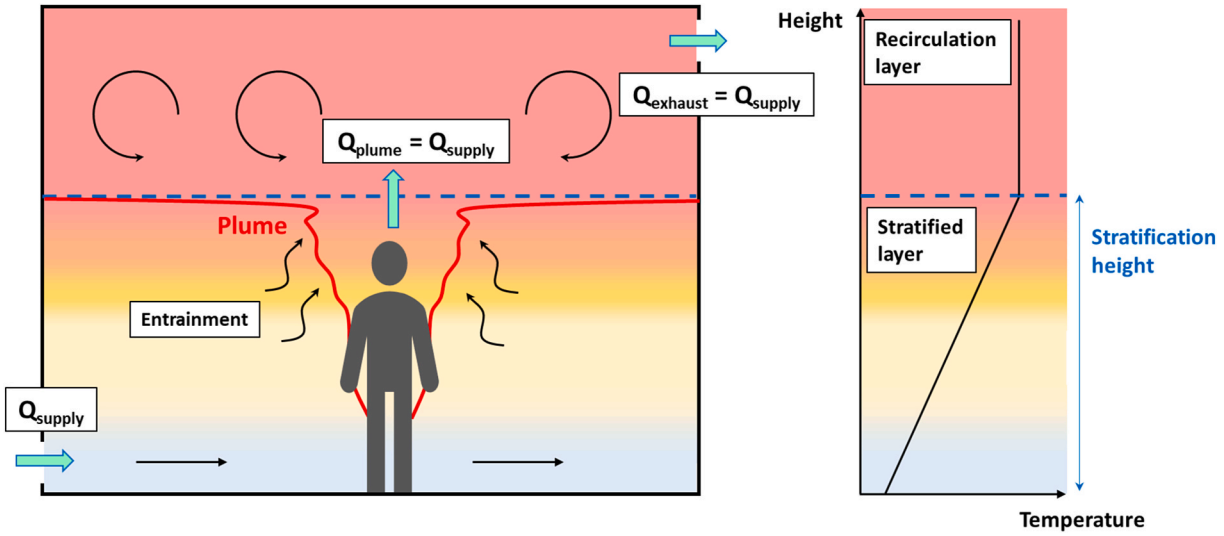

Fig. 3. Typical two-layer thermal field induced by displacement ventilation.

$$Ar = \frac{g\beta h \Delta T_e}{v^2} \quad (4)$$

Where g is the gravitational acceleration, β is the volumetric thermal expansion coefficient of air, h is the room height, ΔT_e is the temperature difference between exhaust and supply air, and v is the characteristic air velocity, given as the ratio of the supply flow rate to the floor area.

The research activities on the thermal characterisation of displacement ventilated rooms aimed at defining the impact of influencing factors on the stratified temperature field. Kosonen et al. [40] studied the effect of single and combined heat gains, showing that the sources' type and position significantly impact steady stratification. Point and distributed heat sources at the floor level produce the typical two-layer stratified space with a marked interface. On the contrary, vertical and roof-level distributed heat sources create a relatively continuous stratification with an almost linear temperature profile along the room height. The temperature gradient is significantly affected by the vertical position of the heat source, whereas its horizontal location has a marginal effect [41,42].

The heat source strength also has a relevant impact on temperature stratification since it drives the flow, impacting stratification and comfort [43]. The stratification interface progressively lowers with higher heat gains in the occupied zone, i.e., higher *Ar* (buoyancy dominant flow) [40,44]. Moreover, warmer rising plumes associated with higher heat sources' powers increase the average temperature and the gradient in the lower zone [37,42].

The supply air conditions, i.e., inlet velocity and temperature, must be properly set to guarantee comfort conditions [36,45,46]. The inlet velocity is associated with the supply flow rate and defines the momentum of the inlet air, while the inlet temperature contributes to enhancing or weakening the buoyancy effect. As the supply flow rate increases, the room's average air temperature and gradient reduce while the stratification layer rises [41,43,47–51], presenting an opposite impact compared to heat source strength. Two experimental studies show that an intermediate stratified layer with a certain thickness appears with high flow rates, both for supply [47] and exhaust DV configuration [49]. Some studies analyse the effect of vents' size in natural DV systems; larger openings are associated with lower aerodynamic resistance and, consequently, higher airflow rates, leading to similar effects [42,44]. On the other hand, higher supply air temperatures entail higher room average air temperatures, lower gradients and lower mixing layers [43,48].

The position of inlets and outlets also impacts the temperature distribution. Ahmed et al. [52] and Gil-Lopez et al. [53] investigated the influence of the exhaust vents' height, suggesting that placing them at ceiling level combined with indoor heat sources, e.g., ceiling lamps, could improve thermal comfort, lowering the average room temperature and vertical temperature gradient. On the contrary, Kosonen et al. [40] analysed the impact of room height, from 3.3 to 5.1 m, on the temperature profile, concluding that with typical heat gains of moderate environments, the vertical temperature gradients occur already in the occupied zone. In these situations, the location of the exhaust vent seems to have a negligible effect on the temperature field and interface height. Cheng et al. [54] considered installing a middle-level return grille separated from the ceiling exhaust outlet for energy-saving purposes. They found out that the height of the return opening has a marginal influence on the temperature profile as long as it is maintained above the occupied zone, with a slight increase in the vertical gradient between head and feet if lowered. Liu et al. [50] compared a low-level side inlet and a floor vent in a naturally displacement ventilated space. The supply air spreads over the floor in the wall inlet case, leading to an average room air temperature of 1–1.5 °C lower in cooling conditions, improving perceived comfort. Yang et al. [51] showed that the interface layer is lower when the inlet and the ceiling exhaust are placed on the same side (i.e., single-sided ventilation) compared to a cross-ventilation configuration, whereas the vertical temperature gradient in the occupied zone remains almost unaffected.

The importance of accounting for radiative heat exchange when dealing with DV systems is also highlighted. Gil-Lopez et al. [53] stress that the heat transfer from ceiling to floor should be considered when sizing the ventilation system, especially for high spaces, e.g., airport terminals. Ceiling temperature rises if warm air stagnates close to it, leading to adding thermal radiative load that must be offset. Menchaca-Brandan et al. [55] numerically verified that the operative temperature is inaccurately estimated if thermal radiation contribution is neglected: the predicted air temperature in the occupied zone results 2–4 °C lower, whereas the surface temperatures of heat sources are up to 17 °C higher. Le Dréau et al. [56] investigated the convective heat transfer during DV night-time operation, showing that low floor emissivity reduces the radiative flux from the ceiling, which is redistributed to the other surfaces, involving a reduction of the convective exchange between floor and air.

People's movements are critical for a ventilation system which exploits the presence of heat sources and is tailor-designed for a specific room layout. Moving heat gains inevitably affect the airflow and temperature distributions. Wu and Lin [57] highlight that short-time walks do not significantly disturb the thermal environment, while long-time movements induce a relevant mixing effect, reducing the steady temperature stratification produced by DV. In the latter case, the walking route parallel or perpendicular to the DV supply jet has a minor influence on the level of produced disturbance. For continuous movement, the higher the walking speed, the stronger the mixing effect [58]. Fen et al. [59] conclude that only the area around the moving heat source is significantly affected, and higher ventilation flow rates smooth the effect. The time required to restore the steady-state stratification increases with walking speed and duration.

Some works compare the performance of DV, stratum (SV) and mixing ventilation (MV). The main issue for DV regards the potential discomfort caused by vertical temperature differences, while the other two provide lower gradients in the occupied zone [36]. According to a study from Cheng et al. [46], DV produces a slightly cool environment with a lower PMV than MV at the same supply conditions. Similarly, Fong et al. [45] by conducting thermal comfort surveys on 48 subjects in a medium-sized classroom in Hong Kong, obtained that reducing the flow rate from 15 to 10 ACH (air changes per hour) improves the acceptability percentage with DV. Wu et al. [57,58] proved that DV is the most sensitive to dynamic phenomena affecting the indoor environment, e.g., people's movements, since it needs more time to recover steady-state conditions after long-duration disturbances stop.

An increasing interest is oriented towards DV integration with radiant heating or cooling systems. In general, stratified air distribution systems are more sensitive to the presence of radiant surfaces [60]. Heating ceilings and cooling floors must be carefully designed when combined with DV since thermal stratification enhances worsening comfort conditions. On the other hand, good compatibility is obtained by coupling DV to a cooling ceiling (CC/DV) or heating floor (HF/DV). However, the former produces cool downward airflow, hindering the typical upward buoyant plumes driving DV, whereas the latter could cause short-circuiting of inlet air if the surface temperature is not properly set. Therefore, the design phase of these systems is challenging, and the combined interactions must be considered. In this panorama, the coupled CC/DV system is a mature technology developed to increase the cooling capacity of DV, which is limited due to thermal comfort constraints. The overall temperature distribution is determined by the balance of DV-upward and CC-downward airflow motions and the ratio of the cooling loads respectively removed based on ceiling surface temperature [61]. Besides radiant systems, DV can be effectively combined with convective hydronic systems such as passive chilled beams (PCBs) [62–64]. Table 1 presents a summary of recent studies on coupled systems.

3.2. Airflow field

The DV steady operation is influenced by multiple airflow elements, as shown in Fig. 4. The overall flow field is determined by the supply air jet, the thermal plume and the associated air entrainment, recirculation motion above the stratification height and downdrafts along cold vertical surfaces.

Low-side diffusers supply fresh air at low inlet velocity and a temperature slightly below the room average. In this way, the negative buoyancy effect flattens the inlet jet that spreads over the floor as a gravity current [71]. The DV jet is typically decoupled into a primary zone, where the air speed increases due to buoyancy action, and a secondary zone, where the air stream decelerates. Magnier-Bergeron et al. [72] propose a 3D model for calculating the air speed in the secondary zone and the jet thickness variation at increasing distance from a flat wall-mounted DV diffuser. Li et al. [73] experimentally studied the curved surface jet flow from a semi-cylindrical DV diffuser. They proposed a simplified model for calculating the primary zone's length and the secondary zone's airflow temperature. Data show that initial length increases and jet temperature decreases with a higher supply flow rate. Fatemi et al. [74] experimentally studied the flow physics of the non-isothermal jet stream from a large quarter-round corner-mounted DV diffuser. They show that the jet stream can be subdivided into four distinct regions (Fig. 5) where the different magnitudes of inertia, buoyancy and viscous forces drive the flow development. The temperature in the jet increases with distance from the diffuser due to heat exchange with the floor and mixing with warmer room air in the convective and fading zones. Fernandez-Gutierrez et al. [75] formulated correlations, in terms of non-dimensional parameters, related to the convective heat transfer between an isothermal floor and a cool air

Table 1
Summary of studies analysing the thermal environment produced by DV coupled to hydronic systems.

Reference	Coupled system	Method	Focus	Main results
Rees and Haves [65]	Cooling ceiling (CC)	Experimental	CC chilled water supply temperature	- The decrease in the chilled water supply temperature and ceiling temperature, accordingly, involves a decrease in the overall vertical gradient - Recirculation and mixing airflows in the upper part of the room seem to be mainly related to the strength of heat sources' thermal plumes rather than the ceiling cooling capacity (i.e., surface temperature)
Yang et al. [66]	Cooling ceiling (CC) Cooling floor (CF) Cooling wall (CW)	CFD	Effect of cooling system configuration on temperature distribution and comfort	- Configurations with upper cooling surfaces (e.g., ceiling) provide better thermal comfort, reduce the vertical temperature gradient meeting the standards, and maximize the cooling capacity of the whole system
Krajčik et al. [67]	Cooling floor (CF)	Experimental	Temperature distribution with DV and CF/DV	- The presence of the cooling floor increases the vertical air temperature gradient compared to the standalone DV
Krajčik et al. [68]	Cooling floor (CF)	Experimental	Temperature distribution with CF/DV	- Increasing the proportion of cooling load removed by CF, the head-feet temperature difference reaches 6–7 °C
Wu et al. [69]	Heating floor (HF) Heating ceiling (HC)	Experimental	Temperature distribution with DV, DV/HF and DV/HC	- Heating floor configuration similar to standalone DV - Heating ceiling worsens the vertical temperature gradient up to 1 °C on average compared to standalone DV
Wu et al. [70]	Heating floor and ceiling (HFC)	Experimental	Temperature distribution with DV/HCF	- The simultaneous use of heating ceiling and floor increases the vertical gradient compared to DV/HF
Shan and Rim [62]	Passive chilled beams (PCB)	CFD	Percentage of load removed by PCB	- Increasing PCB cooling output fromVia Venezia 1–35131 33–53 % of the total load reduces the head-feet temperature difference from 4 to 1.5 °C due to mixing airflow motion
Shi et al. [63]	Passive chilled beams (PCB)	CFD	Percentage of load removed by PCB	- Increasing the PCB cooling output from 0 to 40 % reduces the vertical temperature gradient towards acceptable values; a slightly cool space due to mixing airflow is created if the increase reaches 80 %
Shi et al. [64]	Passive chilled beams (PCB)	CFD	Percentage of load removed by PCB	- The vertical temperature gradient is negatively correlated to the PCB cooling output

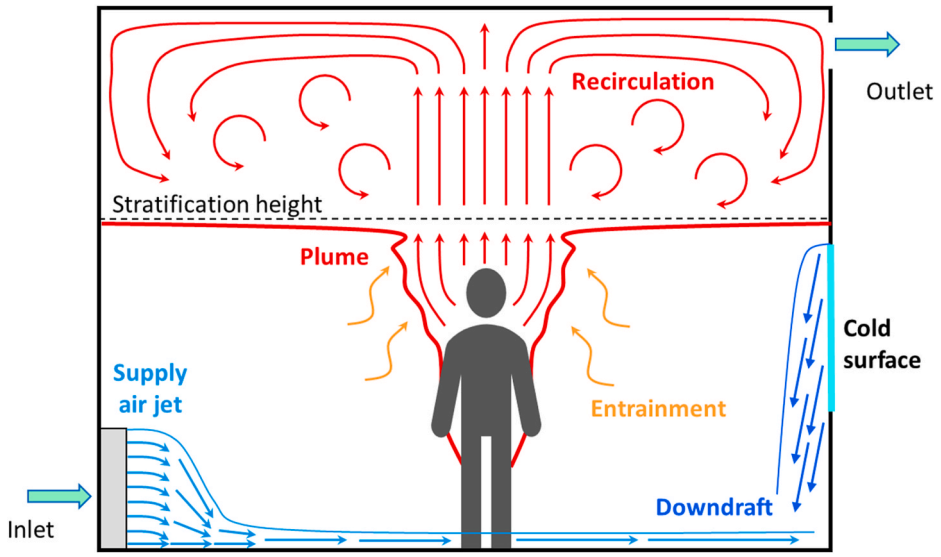

Fig. 4. Airflow elements involved in the steady operation of the DV system.

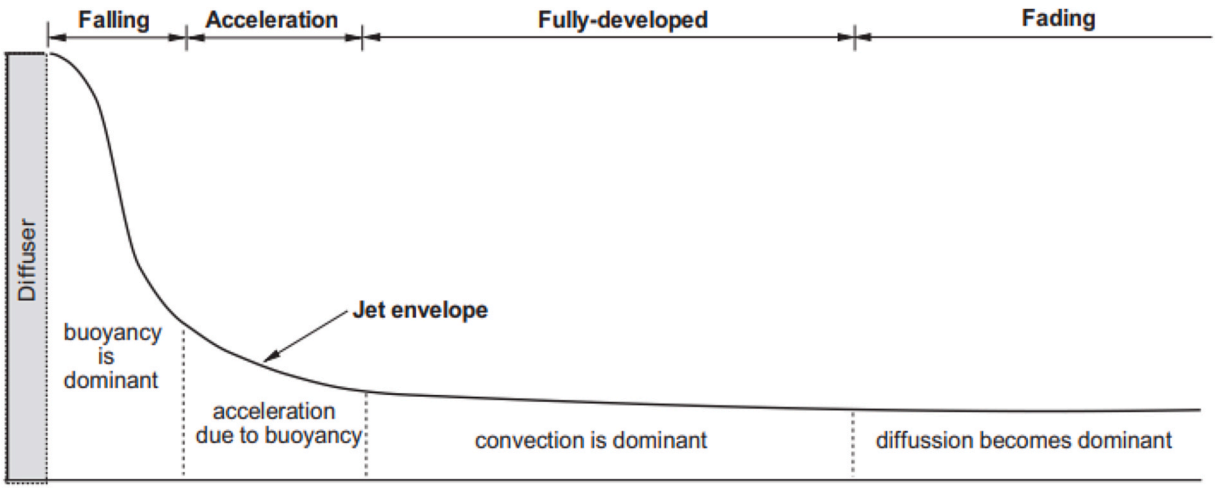

Fig. 5. Regions characterising the development of the DV jet stream (taken from Ref. [74]).

jet from a low-velocity cylindrical DV diffuser in an undisturbed environment. Considering an incompressible, steady-state and laminar flow, they concluded that heat transfer is more sensitive to the temperature difference between inlet and ambient air than flow rate variations.

Incoming fresh air heats up and rises in the form of thermal plumes encountering the heat sources [38]. The buoyant plumes increase their volume flow rate by entraining the surrounding air. Recirculation and mixing occur above the stratification height and are generated by thermal plumes impinging on the ceiling and re-descending towards the occupied zone up to the interface level (see Fig. 4).

Cool vertical surfaces generate downdrafts that hinder the buoyant rising flow and disturb the DV operation. If the cold surface temperature decreases, the downdraft rate increases, inducing a mixing effect that disrupts thermal stratification, especially if the internal heat gains are weak [76]. On the contrary, warm vertical surfaces produce upward airflows in the form of rising thermal plumes and affect the steady stratified environment [41,76].

The steady displacement flow depends on the balance of these airflow elements. However, other dynamic phenomena of moderate extent or short duration can affect the DV flow. Inhalation and exhalation, characterising the human respiratory cycle, significantly impact the flow and temperature field in the subject's breathing zone [38]. The nose breathing mode can disturb the convective boundary layer around the human body and the development of the thermal plume, which reduces its peak velocity above the subject's head [77]. Furthermore, people's movement generates a wake flow behind the individuals' backs. Wu and Gao [78] obtained that for motion speed below 0.2 m/s, the thermal plume and wake flow have comparable strengths, while for walking speed higher than 0.4 m/s, the wake flow becomes dominant; at 1 m/s, it causes an intense mixing disturbing the displacement flow.

The air velocity distribution around the human body is critical to localised thermal discomfort. Indeed, high-speed values associated with cold airstreams may cause draught risk due to undesired convective cooling at specific susceptible body parts, e.g., neck and ankles [13,14]. Standards typically suggest a maximum velocity of 0.2 m/s in the occupied space of moderate environments. The draft rate (DR) is the percentage of occupants predicted to perceive discomfort due to air movements, according to Standard ISO EN 7730 [14].

Draft risk is a significant issue related to DV operation. Indeed, fresh air is supplied at a low temperature directly to the occupied zone at floor level. Despite the typical low inlet velocities, the cold stream over the floor may cause discomfort at foot level, especially near the DV diffuser. Close to the inlet, the air velocity at ankle level (0.1 m from the floor) generally settles between 0.1 and 0.2 m/s [36,46,69,79,80], and a well-design system guarantees a draft rate below 20 % [36,37,46,80], for which the ventilated space is in class B comfort category according to ISO EN 7730 [14]. In the rest of the occupied zone, a one-dimensional displacement flow develops at moderate velocities driven by buoyancy, and at the head level, the draught risk is irrelevant. The velocity field does not present horizontal gradients except in the jet area along the floor [36,79,80]. Compared to other air distribution systems, the DV flow field is characterised by smaller velocity fluctuations in the occupied zone and generally guarantees lower draft risk [36,37,46,69,80]. On the contrary, experimentally studying the draft sensation at ankles for women, Schiavon et al. [81] found that the percentage of dissatisfaction with air movement could reach 57 %, highlighting the importance of designing specific guidelines for localised comfort in a displacement ventilated space. However, the survey campaign was attended by women keeping their ankles uncovered, and some tests were carried out at supply velocities up to 0.7 m/s, which are unusual for a DV system; for typical inlet velocities, the unacceptability rate was reduced to 23–33 %. Ahn et al. [82] investigated the flow field induced by DV serving two adjacent rooms connected by an open door and obtained that air velocity at ankles could reach 0.35 m/s, leading to a DR up to 26 %.

The integration of hydronic systems modifies the DV airflow distribution based on the considered configuration. Cooling ceiling and passive chilled beams (PCB) are responsible for a mixing effect in the upper part of the room, which is characterised by higher velocities [62,63,65]. The larger the cooling output from the PCBs, the higher the occupied zone is affected, with mean air velocity and DR generally remaining in the acceptability range [62,63]. However, Shi et al. [63] shown that if the number of installed beams is low, the DR in the occupied zone could exceed 30 % when the PCB cooling share becomes high (e.g., 80 %) due to strong vertical downdraughts directly below the devices. A cooling floor configuration is beneficial in terms of DR since the air velocity at the ankle level decreases if the cooling load is gradually allocated from DV to the CF system while the occupied zone remains almost unaffected [68]. The presence of a heating floor enhances the air velocities and turbulence intensity in the occupied zone, whereas a heating ceiling preserves the flow field of the standalone DV system [69,70].

Combining temperature and velocity distribution related to DV operation, the overall thermal conditions in the room can be described by defining the local Effective Draught Temperature (EDT) according to Eq. (5) [10,80].

$$EDT = \left(T_{a,loc} - T_{a,avg}\right) - 8\left(v_{a,loc} - 0.15\right) \tag{5}$$

Where $T_{a,loc}$ is the local air temperature, $T_{a,avg}$ is the spatial average air temperature in the occupied zone and $v_{a,loc}$ is the local air velocity. The Air Diffusion Performance Index (ADPI) is calculated through Eq. (6) from the EDT [9,10,46,80] to evaluate how the ventilation system affects the thermal environment and comfort conditions. It indicates the percentage of points in the occupied zone that fall within the acceptability range of EDT, i.e., between −1.7 and 1.1 °C [80].

$$ADPI = \frac{N_{-1.7°C<EDT<1.1°C}}{N} * 100 \tag{6}$$

DV generally produces a higher non-uniformity of the thermal environment than other air distribution strategies, with ADPI values varying between 25 % and 80 % [46,80].

3.3. Indoor air quality and ventilation effectiveness

The primary purpose of ventilation systems is to preserve indoor air quality by providing fresh air to the occupied zone to replace stale air. Indoor pollutants can be generated by active or passive sources. The formers are those associated with heat sources, e.g., human subjects emitting CO_2, whereas those not connected to heat generation, e.g., building fabric and furniture, are passive sources responsible for the release of polluting substances such as volatile organic compounds (VOCs) [10,61]. Indoor pollutants can be differentiated into gaseous contaminants, like CO_2, and particles (both liquid and solid), such as particulate matter. Their nature affects the interaction with room airflow and their transport since heavier particles undergo gravitational sedimentation, while gases' spread normally follows the air motion. The recent COVID-19 pandemic has increased the concern for the airborne transmission of respiratory diseases. The exhaled virus-laden droplets shrink due to evaporation, and the resulting microdroplets behave like small infectious particles. In this context, ventilation is also fundamental to diminishing the airborne infection risks in indoor occupied spaces [22–24].

Indoor air quality in enclosed environments is determined by the distribution and concentration of contaminants. The transport of pollutants is strictly related to the airflow distribution in the space produced by the background ventilation system. Mixing ventilation is designed to produce strong recirculation in the room and dilute the contaminant concentration. Instead, DV exploits the heat sources to create an overall low-momentum upward airflow that displaces the contaminants towards the ceiling, physically removing them.

The indoor air quality in a displacement ventilated space can be described using different indicators. Table 2 reports the indexes typically used in literature and their expressions (Eqs. 7-15).

Several studies investigate the level of IAQ achieved during the operation of a DV system. Both CFD modelling [51,52,62–64,78,82,83,89–94] and experimental approach [31,36,41,57,58,68–70,76,84,87,88,95,96] have been widely adopted. Typically, CO_2 is used

Table 2
Main indicators used in literature to define the Indoor Air Quality in a ventilated space.

IAQ aspect	Parameter	Meaning and notes	Equation	
General indicators	C	Local contaminant concentration - measured data in experimental set-ups or simulated values from CFD analyses	–	
	$\overline{C}$	Average spatial contaminant concentration - calculated for the whole space or a target zone	$\overline{C} = \frac{\sum_{i=1}^{N} C_i}{N}$	(7)
	C_{norm}	Normalized contaminant concentration [41,63,83] - local concentration is normalized on that at the exhaust (C_{exh})	$C_{norm} = \frac{C - C_{supply}}{C_{exh} - C_{supply}}$	(8)
Ventilation effectiveness	ε_c	Contaminant Removal Effectiveness (CRE) [10,16,18,36,84,85] - the ability of the ventilation system to remove the airborne contaminants or how quickly they are exhausted	$\varepsilon_c = \frac{C_{exh} - C_{supply}}{C - C_{supply}}$	(9)
	τ	Age of air [9,10,18,63,84,86,87] - the local mean age of air (τ_p or MAA) is defined as the average time required for the supply air to travel from the diffuser to a given point p in the room - the age of air expresses the freshness of the room air (average value $\overline{\tau}$) - MAA is governed by a transport equation that can be solved through CFD - MAA can be determined experimentally through the tracer-gas decay technique	$\tau_p = \frac{\int_0^{\infty} C_p(t)\mathrm{d}t}{C(0)}$	(10)
	ε_a	Air Change Efficiency (ACE) [10,16,84,87,88] - it describes how quickly the room air is replaced by fresh air - the local value ($\varepsilon_{a,p}$) is a function of the local mean age of air and the room nominal time constant τ_n, reciprocal of the air change rate (ACH)	$\varepsilon_a = \frac{\tau_n}{2\,\overline{\tau}}$ $\varepsilon_{a,p} = \frac{\tau_n}{\tau_p}$	(11) (12)
Exposure and infection risk	C_{inh}	Inhaled contaminant concentration [41] - it includes the air entrainment by the human plume up to inhalation height h_{inh}	$C_{inh} = \frac{\int_0^{h_{inh}} Q_{entr}(y)C(y)\mathrm{d}y}{Q_{plume}(h_{inh})}$	(13)
	ε_{exp}	Personal exposure index [6,16] - a function of the contaminant concentration in the inhaled air	$\varepsilon_{exp} = \frac{C_{exh} - C_{supply}}{C_{inh} - C_{supply}}$	(14)
	IF	Intake fraction [6,88] - fraction of the exhaled pollutants that are inhaled by a susceptible subject in the exposure time	$IF = \frac{\int_0^{t_{exp}} Q_{inh}\, C_{inh}\mathrm{d}t}{\int_0^{t_{exp}} Q_{exhal}\, C_{exhal}\mathrm{d}t}$	(15)

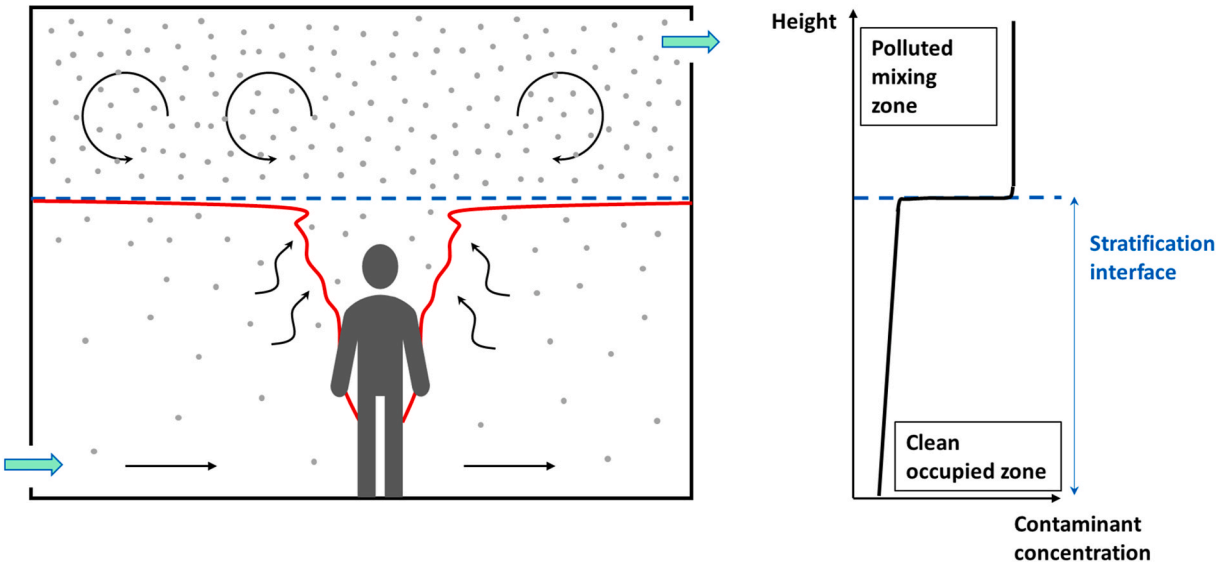

Fig. 6. Ideal contaminant distribution and concentration profile during DV operation.

as an air quality marker representing gaseous or light contaminants [36,41,51,57,58,68,76,84,94,96]. Otherwise, tracer gases are used as surrogates, e.g., SF_6 [62–64,82], freon [69,70], N_2O [95] and others [78,88]. Particles and droplets are also generated in research focussed on heavier contaminant transportation [31,52,83,87,89–92,97] to account for the influence of the gravity force. Similar to the vertical thermal gradient, a contaminant stratification is obtained when DV operates, in the case of buoyant gaseous pollutants, e.g., CO_2. The concentration variation at the stratified interface is sharper than the temperature profile, with a more evident discontinuity between lower and upper zones [41,51,76,96]. The upward flow around the heat sources pushes the pollutants towards the ceiling above the stratification layer (see Fig. 4). If the DV system is well-designed, the recirculation zone should not interfere with the occupied zone. Fig. 6 shows the optimal pollutant distribution and concentration profile with DV, consisting of a lower clean zone with a small concentration gradient and an upper polluted zone where transported contaminants accumulate and mix up. Pei et al. [94] suggest that CO_2-based demand control DV should be managed by placing CO_2 sensors at head level rather than in the exhaust to not overestimate the CO_2 concentration at the breathing zone due to contaminant stratification.

The effectiveness of DV in providing good air quality is mainly influenced by the relative position between contaminant and heat sources, i.e., the presence of active or passive contaminant emitters. DV performs better when the pollution source is the occupant's armpit rather than a floor point; in the first case, the contaminant removal effectiveness (CRE) in the occupied and breathing zone lies between 1.4 and 1.8, whereas it ranges between 0.9 and 1.34 with the passive source [36,84]. Alotaibi et al. [91] suggest that DV badly removes re-suspended particles from the floor, whereas it is effective when dealing with human generation at the breathing level. Moreover, the relative strength and position between active polluting sources and other heat sources are crucial in determining the contaminant transportation since the weaker thermal plumes may be prevented from reaching the ceiling by the more intense ones [16,41,89]. Pei et al. [94] suggest that a higher number of active sources, e.g., occupants, exacerbates the vertical CO_2 concentration gradient with a lower interface height.

The effect of gravitational sedimentation has also been investigated on the transport of heavier pollutants. The tendency of larger particles to settle on the floor hinders the low-momentum displacement flow pushing the contaminants upwards. Mingotti and Woods [31] conducted salt-bath experiments with an active particle source, observing the particles accumulate just above the interface at a low flow rate, and a decreasing concentration gradient occurs up to the exhaust vent, leading to a stratified upper layer. Larger particles are not extracted and rapidly settle on the floor across the interface. The settlement of larger particles enhances their deposition rate and lowers the concentration interface, increasing the pollutants' presence at the breathing level and the intake fraction [76,83]. Studying the transport of virus-laden droplets in the context of the COVID-19 pandemic, Carlotti et al. [92] show that aerosolised particles above 50 μm diameter rapidly sediment close to the infected source, whereas middle-size ones have longer lifetimes and travel further.

The increase in the ventilation flow rate generally lifts the concentration interface and improves the air quality in the occupied zone [41,51], enhancing the possibility of venting the larger particles [31,90,97]. A better ability to provide fresh air to the occupied zone is observed by increasing the flow rate, i.e., lower age of air and higher air change efficiency (ACE) [87,98]. On the other hand, Berlanga et al. [88] suggest that an increase in the supply flow rate from 6 to 9 and 12 ACH does not guarantee a direct improvement in all the IAQ indices in hospital airborne infection isolation rooms (AIIRs). Similar outcomes are drawn with 6 and 12 ACH, whereas the 9 ACH scenario entails better ACE and IF values and worse CRE.

The relative position between pollutant sources and DV inlet and outlet vents is also important [87,99]. Ahmed et al. [52] suggest that combining the exhaust vent with the ceiling light slots provides better air quality in the breathing zone. Studying DV serving two connected rooms, Ahn et al. [82] show that fresh air should be supplied to both to have a lower mean age of air and a higher ACE for the

breathing zone averaged on the whole space. Analysing the removal of particles, Cetin et al. [90] obtained that single-sided DV, i.e., diffuser and exhaust vent on the same wall, generally provides better ACE (in the range 0.51–0.57) and CRE values (between 0.8 and 3.50) compared to crossflow configurations in most situations. The opposite result was obtained by Yang et al. [51].

Several works analyse the *lock-up* phenomenon, for which the contaminants remain trapped and accumulate below the stratification height at the breathing level. During DV operation, it can occur for two reasons. On one hand, the contaminant generation is associated with the weakest heat sources in the space [41,88]. In the second instance, exhaled pollutants could escape the body's thermal plume due to the breathing flow momentum [100]. Zhou et al. [95] experimentally verified that continuously exhaled air oscillates up and down at a certain height in a thermally stratified environment, and the lock-up height is negatively correlated with exhalation velocity and decreases with larger vertical temperature gradients. Some authors point out that the rising convective boundary layer around the human body may protect occupants from the background locked-up concentration, bringing fresh air from the bottom to the inhalation zone [41,88].

The contaminant distribution is strongly affected by airflow disturbances. Investigating the interactions between thermal plume and walking wake flow, Wu and Gao [78] stated that a walking speed of 1 m/s makes the pollutants spread horizontally and vertically in a mixing process. Moreover, the recovery of contaminant distribution is much slower than the airflow field after the movement stops. The previous findings are confirmed by two works of Wu and Lin [57,58], which also underline that short-time movements have a marginal impact on CO_2 distribution. Two similar studies on DV in hospital wards [41,76] highlight that upward plumes along warm walls may cause stagnation (lock-up) depending on the active pollution sources' strength, whereas downdrafts along cold surfaces bring pollutants towards the occupied zone, lowering the IAQ; the latter effect enhances the larger the temperature difference between air and surface is.

The research on integrated HVAC solutions coupling DV to other systems has also focussed on how their interaction affects IAQ. No significant differences are observed between standalone DV and DV combined to heating floor or ceiling [69,70]. Shan et al. [62] obtained that, raising the PCB cooling output from 33 to 53 % of the total load, the age of air approximately increases from 0.15 to 0.2 h in the breathing zone, and accordingly, the DV ventilation effectiveness worsens with ACE decreasing from 1.6 to 1.2. Similar outcomes were obtained in Refs. [63,64].

Several studies investigate the advantages in improving IAQ compared to other air distribution strategies, especially the widespread MV systems. Table 3 reports some works comparing the performance of DV and MV (see Table 2 for the IAQ indices). The table shows that considering the whole ventilated volume, MV achieves an ACE and a CRE of around 0.5 and 1, respectively. On the other hand, DV outperforms MV in both aspects with the same supply flow rate. The same outcomes are observed when focusing on the occupied or breathing zones. Nevertheless, DV also presents some weak points compared to MV. Jurelionis et al. [87] show that DV is rather inefficient in removing particles and measured an average age of air of 16.7 s against a value of 9.9 s for MV at 3–4 ACH. Moreover, DV is more sensitive to disturbances like occupants' long-time movements, which strongly affect contaminant distribution [57,58].

Recently, DV has gained renewed interest in the context of the COVID-19 outbreak as a measure to reduce the airborne infection risk. The virus-laden microdroplets originate from active sources and are effectively brought towards the ceiling and exhausted with a minimised horizontal spread when DV is applied [101]. Replacing MV with DV [99,102,103].

3.4. Energy performance of DV

The energy performance of DV is typically evaluated in comparison to widely used MV systems. Generally, researchers focus on the cooling season, when the DV usage is more effective. Sections 3.1 and 3.2 clearly show that thermal comfort issues related to vertical air temperature gradient and ankle-level draft risk limit the inlet air temperature. However, since DV systems supply fresh air directly to the occupied zone, comfort conditions are also guaranteed at a supply temperature 2–4 °C higher than MV [16]. Moreover, the results presented in Table 3 imply that the same IAQ level can be achieved with a lower supply flow rate in the case of DV. From this point of view, DV has a relevant energy-saving potential. Pei et al. [94] suggest that the CO_2 sensor must be placed at the breathing level rather than at the exhaust when using a demand control DV since the needed flow rate could be overestimated due to stratification; the authors state that a measurement error of 230 ppm in a space with five occupants may yield a power increase of 1200 and 1100 kW for air conditioning and fan operation, respectively.

DV operation permits offsetting only the cooling load of the occupied portion of the room, whereas the ceiling-level heat load is directly discharged at the exhaust. The energy benefits are related to the reduction of the volume that needs to be cooled down. This peculiarity of stratified air distribution systems (STRAD) to decrease the overall cooling coil load in the air handling system is expressed by Eq. (16) [52,54,104,105]:

$$q_{coil,STRAD} = q_{coil,MV} - \rho\, Q_{exh}\, c_p (T_{exh} - T_{set}) \tag{16}$$

Where $q_{coil,MV}$ is the cooling coil load for the MV system with the same setpoint temperature T_{set} as the STRAD system, Q_{exh} and T_{exh} are the exhaust flow rate and temperature. The second term is the load reduction achieved using a STRAD system, representing the unoccupied zone's heat load. According to Ahmed et al. [52], by placing the exhaust vent at the ceiling level and combining it with heat sources, e.g., light slots, an energy saving of up to 25 % is obtained compared to the MV system. On the other hand, Cheng et al. [54] suggest installing a separate return vent at the upper boundary of the occupied zone to reduce the cooling load from 15 to 21 %.

Ventilation performance in providing cooling is often expressed through the heat removal effectiveness (HRE), defined by Eq. (17) for the occupied zone [37,43,80]. It can also be determined for a specific point in the space [85] and represents the ability to remove the sensible load compared to the well-mixing case, whose reference value is unitary.

Table 3
Summary of works comparing the performance of DV to MV in terms of IAQ ("bz" stands for breathing zone, "oz" for the occupied zone, and no subscripts for the whole space).

Reference	DV	MV	Notes
Krajčik et al. [68]	$\varepsilon_{a,bz} = 1.49$	Ref. values	- Values given for a flow rate of 1.5 ACH
	$\varepsilon_{a,1.7m} = 1.06$	$\varepsilon_{a,bz} = 1$	- DV involves mixing above the interface layer (1.7 m)
	$\varepsilon_{c,bz} = 3.01$	$\varepsilon_{c,bz} = 1$	
	$\varepsilon_{c,1.7m} = 1.16$		
Mateus and Carrilho da Graça [96]	$\varepsilon_{c,oz} = 1.2$	Ref. value	- Values for two case studies, a concert hall and an orchestra rehearsal room
	$\varepsilon_{c,oz} = 1.7$	$\varepsilon_{c,oz} = 1$	
Ahn et al. [82]	$\varepsilon_{a,bz} = 1.62$-$1.78$	$\varepsilon_{a,bz} = 1.1$-1.15	- Two connected rooms with an inlet vent in both supplying a flow rate of 1.5 ACH
	$\tau_{bz} = 12.3$–13.3 min	$\tau_{bz} = 17.3$–18.3 min	
Tian et al. [36]	Armpit pollutant source	Armpit pollutant source	- Flow rate varied between 2.2 and 4.7 ACH
	$\varepsilon_{c,oz} = 1.42$-$1.62$	$\varepsilon_{c,oz} = 0.85$–$1.03$	- DV is less efficient with a passive source (floor) but still provides better IAQ than MV
	$\varepsilon_{c,bz} = 1.35$-$1.57$	$\varepsilon_{c,bz} = 0.86$–$1.06$	
	Floor pollutant source	Floor pollutant source	
	$\varepsilon_{c,oz} = 1.15$-$1.34$	$\varepsilon_{c,oz} = 0.79$-$0.98$	
	$\varepsilon_{c,bz} = 1.19$-$1.27$	$\varepsilon_{c,bz} = 0.81$-$0.91$	
Brockman and Kriegel [98]	$\varepsilon_{a} = 0.65$-0.75	$\varepsilon_{a} = 0.5$-0.6	- Flow rate varied between 2.1 and 8.4 ACH
	$\varepsilon_{c} = 1.35$-1.45	$\varepsilon_{c} = 0.95$–1.2	
Tian et al. [84]	$\varepsilon_{a} = 0.76$-0.84	$\varepsilon_{a} = 0.54$-0.65	- Results for armpit pollutant source
	$\varepsilon_{c} = 1.1$-1.65	$\varepsilon_{c} = 0.85$–1.05	- Flow rate varied between 2.2 and 4.7 ACH
	$\varepsilon_{a,bz} = 1$–1.30	$\varepsilon_{a,bz} = 0.8$–1.10	
	$\varepsilon_{c,bz} = 1.35$-$1.8$	$\varepsilon_{c,bz} = 0.9$–1.1	
Liu et al. [83]	$\varepsilon_{c} = 2.82$–5.52	$\varepsilon_{c} = 0.97$–1.08	- Flow rate varied between 2 and 6 ACH
	$\varepsilon_{c,bz} = 1.07$–$6.05$	$\varepsilon_{c,bz} = 0.97$–$1.10$	

$$\varepsilon_t = \frac{T_{exh} - T_{supply}}{T_{oz} - T_{supply}} \tag{17}$$

Where T_{sup} and T_{exh} are the supply and exhaust temperatures, T_{oz} is the average temperature in the occupied zone. A DV system presents an HRE value higher than 1 due to stratification; the closer T_{oz} is to the supply temperature, the more efficient the system is in cooling down the occupied space. The HRE is positively correlated to the supply flow rate [43]. In the works from Chen et al. [37] and Zhao et al. [80], the DV HRE lies in the range 1.1–1.5 and 1.22–1.36, respectively, decreasing when heat load increases.

With the same supply flow rate, DV is superior to MV in energy performance. Fong et al. [45] run a TRNSYS model to calculate the year-round energy usage. The cooling energy consumption can be reduced by 9.28 and 16.17 % with flow rates of 15 and 10 ACH, respectively, when DV is used instead of MV. In another work [106], a yearly energy saving of 23.38 % is obtained with DV; over 20 years, the CO_2 emissions are reduced by 23.35 %. Ahn et al. [82] determined that DV is two times faster than MV in reaching the setpoint even at a 3 °C higher supply temperature, and this shorter running time enables saving energy. On the other hand, the experimental investigation from Wang et al. [107] shows that DV could be relatively inefficient in the pull-down process without heat sources, i.e., cooling the space prior to occupancy. Liu et al. [79] proved the superiority of DV over MV in a sleeping environment occupied by a lying subject, with energy consumption and exergy losses reduced by around 10 % and 10–20 %, respectively.

4. Simplified modelling approaches for DV

In the panorama of building energy simulations (BES), the multizone modelling approach is widely used in several well-known software (e.g., TRNSYS [108], EnergyPlus [109]). However, they represent each thermal zone as a single perfectly mixed air node, thus not appropriate for describing the stratification produced by DV operation. CFD analysis is a powerful method to capture the complex airflow and temperature distribution in indoor spaces, but it suffers from high computational effort, and numerical simulations can be run for a specific operation scenario at a time with fixed boundary conditions. The review from Tian et al. [110] discusses the coupling between CFD and BES tools. The two approaches can be combined to exploit their strong points and exchange data; nonetheless, the bottleneck remains in the CFD simulation time. Therefore, there is a need for simplified methods to model non-uniform spaces, aiding the DV design phase and improving BES outcomes.

4.1. Analytical and empirical models

The most basic models come from analytical and empirical formulations. The formers are developed from theoretical analysis to describe the physical phenomenon through mass, energy and momentum conservation laws. Generally, they are based on major assumptions that simplify the mathematical framework. On the other hand, empirical expressions are constructed starting from datasets.

The analytical models to describe stratification and the buoyancy-driven upward airflow in displacement ventilated spaces are related to the *emptying filling-box* models. The terminology is associated with the salt-bath experiments usually conducted in parallel to visualize the physical process inside a tank representing an indoor space. These tests employ two liquids with different densities (e.g., pure water and a saline solution) to produce a buoyancy force driving the fluids' motion. The buoyancy effect has been widely studied by arranging different configurations, as illustrated in Fig. 7. The *emptying-box* systems in Fig. 7(a) are used to determine the draining

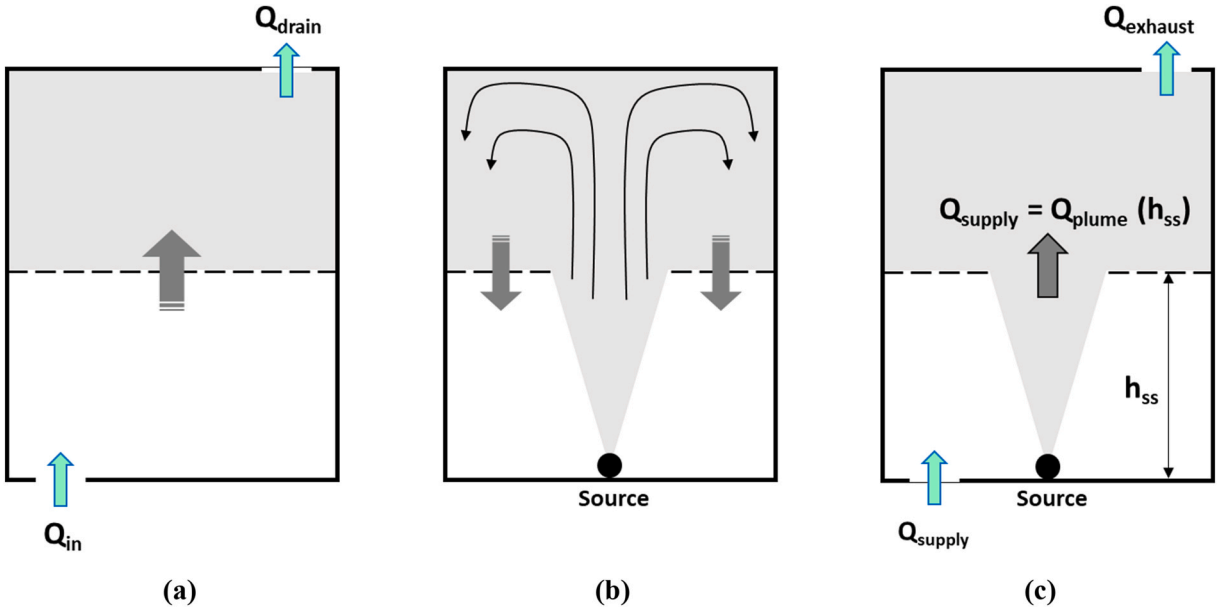

Fig. 7. Different buoyancy flow configurations associated with analytical models. Emptying or draining-box (a), filling-box (b), emptying filling-box (c). The grey region represents the buoyant lighter fluid; the dashed line is the interface between the two layers at different densities.

time of lighter fluid filling the tank with no active buoyancy sources [111]. The *filling-box* systems in Fig. 7(b) investigate a source's buoyant plume behaviour without ventilation. Fig. 7(c) shows the *emptying filling-box* model at steady-state conditions. This last case represents the DV operation with the contemporary presence of a continuous buoyancy source (e.g., a heat source) [30].

Various analytical formulations associated with the system in Fig. 7(c) have been developed to study both natural and mechanical DV, describing either transient and steady-state airflow and stratification. The DV analytical models are based on plume theory from Morton et al. [112]. The buoyancy effect is studied considering the densities rather than the temperatures, but the parameters are strictly correlated. The two layers are assumed to be homogeneous in terms of density and, thus, temperature when applied to a real ventilated room case. Moreover, they consider the lower zone at the same density as the outdoor environment. These analytical models aim to calculate the stratification interface location in the space; at a steady state, it settles at an equilibrium level (h_{ss}) where the plume flow rate matches the inlet flow rate, as expressed in Eq. (18).

$$Q_{plume}(h_{ss}) = Q_{supply} \tag{18}$$

The plume flow rate increases along the vertical direction due to air entrainment in the lower zone. It is expressed for a point source through Eq. (19) [112]:

$$Q_{plume}(h) = C_{pl}\, B^{\frac{1}{3}}\, h^{\frac{5}{3}} \tag{19}$$

Where C_{pl} and B are the plume constant and the source buoyancy flux, respectively, the former is a function of the entrainment coefficient α (Eq. (20)), and the latter depends on the heat source power W (Eq. (21)).

$$C_{pl} = \frac{6}{5}\, \alpha^{\frac{4}{3}}\, \sqrt[3]{\frac{9}{10}}\, \pi^{\frac{2}{3}} \tag{20}$$

$$B = \frac{g\beta W}{\rho c_p} \tag{21}$$

With β as the volumetric thermal expansion coefficient of air, g is the gravity acceleration, ρ the air density, and c_p is the air specific heat at constant pressure.

In the case of mechanical DV, the steady state interface level is obtained with Eq. (22) [47]:

$$h_{ss} = \frac{{Q_{supply}}^{\frac{3}{5}}}{{C_{pl}}^{\frac{3}{5}}\, B^{\frac{1}{5}}} \tag{22}$$

In the case of natural DV, the ventilation flow rate is a function of the stack effect, dependent on the interface height itself and the density of the upper layer, as well as fluid dynamic resistances at inlet and outlet vents. Eq. (23) can be used to calculate h_{ss} with natural DV [30].

$$\frac{A^*}{H^2} = {C_{pl}}^{\frac{3}{2}} \left[\frac{\left(\frac{h_{ss}}{H}\right)^5}{1 - \left(\frac{h_{ss}}{H}\right)} \right]^{\frac{1}{2}} \tag{23}$$

Where H is the room height and the total effective opening area A^* takes into account the effect of head turbulent losses (discharge coefficient C_d) and flow contraction (coefficient C_e) at the vents, as Eq. (24) states [113].

$$A^* = \frac{A_b A_t}{\left[\frac{1}{2}\left(\frac{{A_b}^2}{{C_d}^2} + \frac{{A_t}^2}{{C_e}^2}\right)\right]^{\frac{1}{2}}} \tag{24}$$

Where A_t and A_b are the top and bottom opening areas, respectively.

The most recent research has proposed further developments, starting from the basic framework presented above. The plume theory is accurate enough to predict the steady-state interface height for both mechanical [96,114] and natural DV [115]. The model has been extended to study the push-type [113] and pull-type natural DV [47] between two connected spaces, with a point source located in the upstream and downstream enclosure, respectively, and mechanical extraction DV [49]. Nabi et al. [116] used the classical two-layer stratification model to optimise the air inlet conditions to maintain desired comfort conditions in a specified target zone. By comparison with optimised results from CFD simulations, they established that the analytical model is reliable for an intermediate regime with clear stratification. Duan et al. [117] introduce a thermal balance in the upper region to study the transient evolution of fan-assisted natural DV flow in an enclosure with a floor point source and a solar chimney. Their model shows that when the filling-box time is lower than the draining one, the interface lowers below the steady-state level before equilibrium is restored. This phenomenon, known as *overshooting,* is described also by other transient analytical models [118,119]. Yang et al. [118] developed a three-layer stratification model for natural DV with two interfaces and three uniform regions to consider the reduced buoyancy a point

source plume undergoes above the interface, generating a warmer near-ceiling zone. Shrinivas and Hunt [119] also proposed a three-layer model when two non-interacting heat sources of unequal strength drive natural DV; the weakest plume does not reach the ceiling and generates an intermediate layer with two interfaces.

The analytical models based on the plume theory may be useful in the design phase of mechanical DV since the supply flow rate can be adjusted to keep the interface above the occupied zone once the heat source entity is known. In the case of natural DV, it aids the vents' sizing and positioning to guarantee adequate air change rates. However, they are unsuitable for energy and thermal comfort evaluations since they assume the lower occupied zone to be at the same conditions as the inlet air in terms of density and temperature. On the other hand, they may be appropriate for assessments of IAQ since contaminant distribution is more likely to develop into two well-mixed layers compared to temperature (cf. Figs. 3 and 6). Mingotti and Woods [31] used the plume theory to study the transport of polydisperse particle suspension with mechanical DV.

Some empirical models have also been formulated to describe specific features of DV that can be integrated into multi-zone simulation tools. Generally, they consist of correlations drawn from experimental or numerical data through curve-fitting methods. Yuan et al. [120] proposed empirical equations to estimate the vertical temperature difference between head and foot level and the breathing zone's CRE based on the space's heat source distribution. Dominguez et al. [44] formulated correlations for the dimensionless temperature profile from floor to ceiling as a function of the Archimedes number. Zhang et al. [121] present a data-driven model to describe the non-uniform thermal environment induced by DV, which correlates the local air temperatures and velocities to supply and exhaust air temperatures and inlet velocity through a linear and a polynomial equation, respectively. Important empirical relationships are those for calculating CHTCs between air and surfaces, which can improve the accuracy of BES outcomes [56,122].

Although they are simple correlations to be implemented in other more detailed simulation tools, the authors generally stress that the applicability of the empirical models should be restricted to cases with similar features to the starting database and sometimes give a validity range regarding boundary conditions. Therefore, these models suffer from high specificity and are not universally useable.

4.2. Nodal and zonal models

Analytical models cannot define the temperature gradient in the occupied zone. Nodal and zonal modelling approaches have been adopted to describe temperature distribution with DV. In general, they provide reliable predictions of thermal stratification, requiring less computational resources than detailed CFD simulations [40].

Nodal models determine the temperature gradient in the space by defining a certain number of air nodes in the vertical direction. The air temperatures are calculated by solving the heat balances for each node. On the other hand, mass balances are not considered since these basic models assume an ideal vertical upward airflow, with few exceptions. Fig. 8 reports the nodal models' basic schemes,

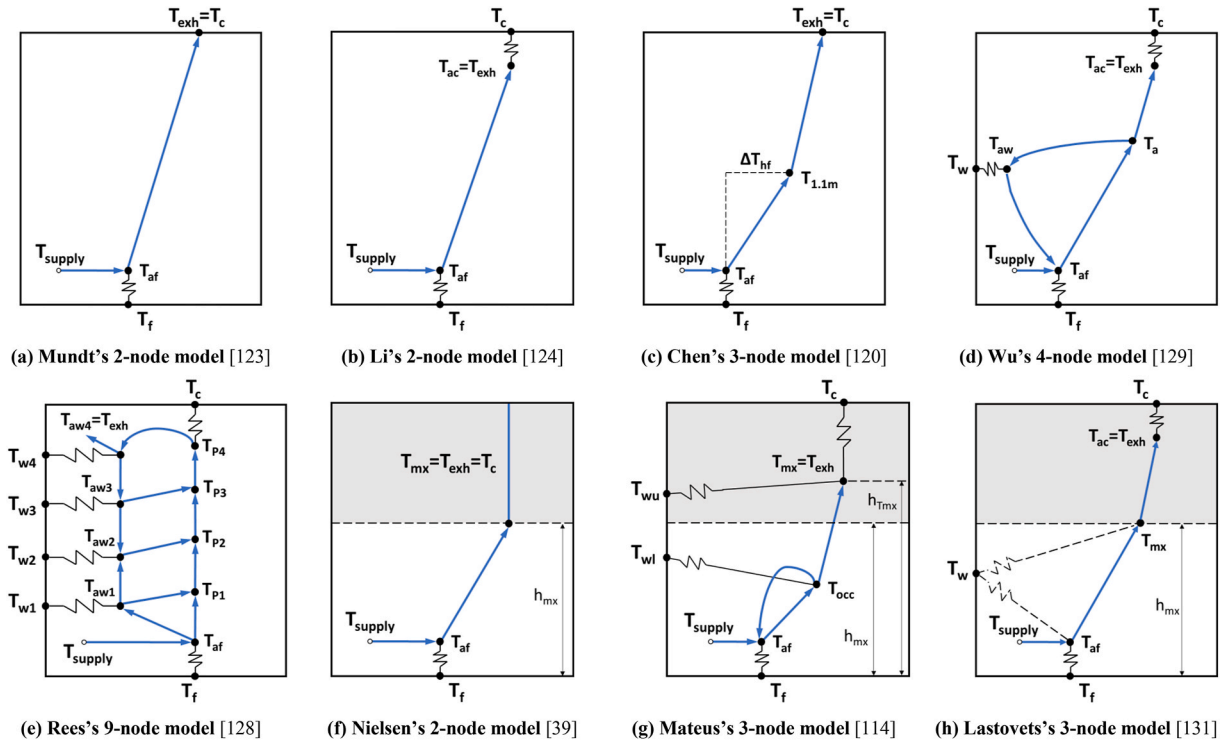

Fig. 8. Simplified DV nodal models for calculation of temperature distribution. The model's name refers to the author and the number of air nodes (except for supply); the grey areas represent the upper layer in the models defining it. (f=floor, c=ceiling, w=wall, exh= exhaust, a=air, occ=occupied, mx=mixing height, P=plume, af, ac, aw = air layer close to floor, ceiling and wall, hf=head-foot).

representing the assumed temperature profile, airflow patterns (blue links), and convective resistances between air and surface nodes. Air temperature is assumed to vary linearly between connected air nodes. Mundt's linear two-node model, shown in Fig. 8(a), was the first conceived [123]. It assumes an air temperature linear gradient over the room height, the exhaust air and ceiling temperatures to be equal, and sets three steady-state heat balances for the whole room (Eq. (25)), for the floor surface (Eq. (26)) and for the node of the air layer 0.1 m above the floor (Eq. (27)).

$$q_{tot} = \rho\, c_p\, Q\left(T_{exh} - T_{supply}\right) \tag{25}$$

$$\alpha_r\, A_f\left(T_{exh} - T_f\right) = \alpha_c\, A_f\left(T_f - T_{af}\right) \tag{26}$$

$$\alpha_c\, A_f\left(T_f - T_{af}\right) = \rho\, c_p\, Q\left(T_{af} - T_{supply}\right) \tag{27}$$

Where q_{tot} is the total room heat load, A_f is the floor area, Q is the volumetric airflow rate, T_{supply} is the supply air temperature, and T_f, T_{af}, and T_{exh} are the unknown temperature of the floor surface, air above the floor and exhaust air. Eqs. (26) and (27) state that radiative heat flux from the ceiling to the floor is transferred to supply air by convection. The convective (α_c) and radiative (α_r) heat transfer coefficients constitute the model's parameters to be specified.

The Mundt's approach underwent several improvements over time. The successive models increase their complexity, gradually including further aspects in the analysis: radiative and conductive heat exchanges, heat gains breakdown, thermal plume modelling, and recirculation airflows. Table 4 reports the contributions given by different researchers in the development process of DV nodal modelling. Despite the differences, all nodal models determine the temperature distribution by solving the steady-state heat balances at each i-th surface and k-th air node, as expressed in a general form by Eqs. (28) and (29), respectively.

$$\sum\nolimits_{j=1}^{n} q_{r,j-i} + q_{c,i} + q_{r,gains} + q_{cond,i} = 0 \tag{28}$$

$$q_{c,sur} + q_{c,gains} = \sum\nolimits_{y=1}^{m} \rho\, c_p\, Q\left(T_{a,k} - T_{a,y}\right) \tag{29}$$

Eq. (28) states that the surface temperature is given by the balance of radiative heat exchange with the other n surfaces, the radiative heat flux from the heat sources, the convective heat exchange with the adjacent air layer and the conductive exchange with the outdoor environment. From Eq. (29), the heat absorbed or released by the airflows coming from the m upstream air nodes (right-hand side) offsets the convective flux from the adjacent surface and the convective fraction of heat gains. Table 4 also shows the main models' parameters with their values or formulations.

Starting from Mundt's model, Li et al. [124] included the convective transfer between the ceiling and the adjacent air layer and conduction through the floor and the ceiling (Fig. 8(b)). The authors also presented a multi-node linear model considering the presence of external walls and the radiative transfer between surfaces. In particular, the wall temperature typically varies with height due to radiative exchanges with the warm ceiling and the cool floor during DV operation; for this reason, the vertical surface can be discretized along the vertical direction into segments with uniform temperature, which exchange heat by convection with the adjacent air nodes. Starting from Li's two-node model, Mundt [125] expressed the radiative heat transfer from the ceiling and toward the floor by including the influence of walls through two corrective coefficients, Y_1 and Y_2. Furthermore, the radiative fraction of heat gains is also taken into account. Li proposed his two-node model as an alternative to classical emptying-filling box models presented in the previous section to study the effect of stratification on the buoyancy-driven natural DV in an enclosure with a point source [126].

Chen's three-node model (Fig. 8(c)) introduces the breakdown of heat gains in relation to the heat sources' positions inside the room [120]. The different allocation of heat load to the occupied and upper zones permits a better representation of the non-linear temperature gradient, which usually settles between floor and exhaust with DV. The model calculates the temperature difference between the head (1.1 m) and feet level (0.1 m) of a seated person through Eq. (30):

$$\Delta T_{head-feet} = \frac{\gamma_{oe}\, q_{oe} + \gamma_l\, q_l + \gamma_{ex}\, q_{ex}}{\rho\, c_p\, Q} \tag{30}$$

Where the heat load q_{oe}, q_l, q_{ex} represent the heat sources located in the occupied zone, the overhead lighting, the heat transmission through structures and incoming solar radiation, while coefficients α_{oe}, α_l and α_{ex} drawn from a significant database of CFD analyses, express their contributions to occupied zone's balance. On the other hand, Arens modifies Mundt's original model by including radiation from all surfaces and the heat sources and convection from a single wall node to a room air node assumed at an average temperature between the floor air layer and the exhaust [127].

Rees and Haves developed a nine-node model (Fig. 8(e)) to calculate the temperature distribution in a room equipped with DV and chilled ceiling [128]. They decouple the heat loads from the bulk room air by inserting special nodes to represent the thermal plumes; the network consists of one floor air node, four plume nodes and four room air nodes. This model provides a first attempt to model thermal plumes, where the convective heat gain is concentrated. Moreover, the assumption of a solely upward airflow is discarded by including air recirculation from the upper nodes and entrainment into the plume. The wall temperature gradient is also considered vertically subdividing the surface into four sections connected to the adjacent room air nodes. Despite its detail level, the model presents some drawbacks. The network topology and the airflow patterns are predefined through CFD analysis or flow visualization, so the model should be adapted to the specific case study. The same occurs for the convection load partition onto the plume nodes. The bulk airflow rates C_i between nodes are precalculated values from experimental data; therefore, the model is difficult to generalise.

Table 4
Summary of nodal model's assumptions and features. (✓ = YES, x = NO).

Reference	Nodal network	Walls included	Surface radiative exchange	Conduction	Heat gains radiative fraction	Heat gains breakdown on air nodes	Recirculation flows	Thermal plume modelling	Model parameters
Mundt, 1990 [123]	Mundt's 2-node	x	✓ ceiling-floor	x	x	x (Eq. (25) for q_{tot})	x	x	$\alpha_c = 3$–5 W m^{-2} K^{-1} $\alpha_r = 5$ W m^{-2} K^{-1}
Li et al., 1992 [124]	Li's 4-node	x	✓ ceiling-floor	✓	x	x (Eq. (25) for q_{tot})	x	x	$\alpha_c = 5$–7 W m^{-2} K^{-1} $\alpha_r = 5$ W m^{-2} K^{-1}
Mundt, 1996 [125]	Li's 4-node	✓ (through Y_1, Y_2)	✓	✓	✓	x (Eq. (25) for q_{tot})	x	x	$\alpha_c = 5$–7 W m^{-2} K^{-1} $\alpha_r = 5$ W m^{-2} K Y_1, $Y_2 = 0.6$-0.8
Yuan et al., 1999 [120]	Chen's 3-node	x	✓ ceiling-floor	✓ (as heat gain to the air nodes)	x	✓ load fraction to the occupied zone (1.1 m node)	x	x	$\alpha_c = 5$–7 W m^{-2} K^{-1} $\alpha_r = 5$ W m^{-2} K^{-1} $\alpha_{oe} = 0.295$ $\alpha_l = 0.132$ $\alpha_{ex} = 0.185$
Arens, 2000 [127]	Mundt's 2-node	✓	✓	x	✓	x	x	x	$\alpha_{c,wall} = 1.5$ W m^{-2} K^{-1} $\alpha_{c,floor} = 4$ W m^{-2} K^{-1} $\alpha_r = 5.8$ W m^{-2} K^{-1}
Rees & Haves, 2001 [128]	Rees's 9-node	✓	✓	x	x	✓	✓ plume air entrainment	✓ plume air nodes	$\alpha_{c,floor} = 2.1$ W m^{-2} K^{-1} $\alpha_{c,ceil} = 5.9$ W m^{-2} K^{-1} $\alpha_{c,wall} = 3$ W m^{-2} K^{-1} $\alpha_{c,w1} = 1.49\ \Delta T_{w1-aw1}^{0.345}$ α_r not specified C_i from CFD [W K^{-1}] (*bulk airflow capacities*)
Nielsen, 1995 [39]	Nielsen's 2-node	x	x	x	x	x (Eq. (25) for q_{tot})	x	✓ h_{mx} calculation	–
Wu et al., 2013 [129]	Wu's 4-node	✓ external and internal separately	✓	✓ external wall	✓	x	✓ downdraft along wall	x	$\alpha_{c,floor}$ = from [132] $\alpha_{c,wall}$ = from [133] $\alpha_{c,ceil} = 0.49\ ACH^{0.8}$ $\alpha_r = 4.7$ W m^{-2} K^{-1}
Mateus & da Graça, 2015 [114]	Mateus's 3-node	✓ above/below h_{mx}	✓	x	✓	✓ above/below h_{mx}	✓ entrainment in the inflow	✓ h_{mx} calculation	$\alpha_{c,i}$ from [132] α_r based on view factors for rectangular cavities $I_M = 0.6$ (*inflow entrainment fraction*) $F_{MO} = 0.4$ (*convective gain mixing in the occupied zone*)
Lastovets et al., 2020 [131]	Lasovets's 3-node	✓ influence on T_{mx} or T_{af} based on h_{mx}	✓	x	✓	✓ above/below h_{mx}	x	✓ h_{mx} calculation	$\alpha_{c,i}$ from [132] $\alpha_r = 5.5$ W m^{-2} K^{-1}

Wu et al. [129] presented a four-node model to determine the temperature gradient achieved by coupling DV to floor heating during winter (Fig. 8(d)). Two air nodes are added to Li's model scheme, one for the room air volume where the convective load impinges and the other for the air layer at the external wall. The downdraft along cold surfaces is calculated in the model and included as a recirculation flow towards the floor air node. Radiation from surfaces and heat sources is also considered. Moreover, the external wall and indoor partition are separated, the former enabling transmission losses towards the outdoors. Based on Wu's model, Zhang et al. [130] employ HRE values to define the thermal field. They propose to correlate the air temperatures at the floor layer, core zone, and ceiling layer to HREs calculated at the corresponding height through empirical formulae, the parameters of which are determined through multiple regression on experimental or numerical data. The idea is that HRE should represent the airflow patterns, avoiding the necessity of knowing precisely the motion field and making it flexible if nodes or heating/cooling systems need to be added; however, the model's generalised applicability must be verified.

Some researchers combined the modelling approach with the plume theory to calculate the interface height of the mixing layer (h_{mx}). Nielsen [39] modifies Mundt's approach, assuming a linear air temperature increase from the floor to the well-mixed layer above the interface (Fig. 8(f)). Moreover, the dimensionless floor surface temperature is directly correlated through the type and distribution of the heat sources through the Archimedes number.

Mateus and da Graça [114] developed the three-node model shown in Fig. 8(g). The air temperatures at the floor layer, the occupied zone (0.6/1.1 m for a seated/standing person) and the mixing layer are calculated; the air mixing node is supposed to be higher than the stratification level calculated through plume theory. Air entrainment in the inflow and the breakdown of the convective load between the occupied zone and upper layer are considered through parameters I_M and F_{MO}. Radiative heat exchange between surfaces and heat sources is included, and the vertical wall is split into upper and lower sections above and below the mixing interface, which are connected to the corresponding air nodes. The model also predicts the temperature distribution well with coupled CC/DV systems [134], although the load breakdown needs to be adjusted, as well as natural DV [115]. It can suitably simulate the DV performance in large rooms, where thermal plumes from close point sources may coalesce, generating linear or planar plumes [96]. Lastovets et al. three-node model gives more importance to load spatial distribution within the ventilated room [131]. As shown in Fig. 8(h), the upper layer above the calculated interface is not considered as perfectly mixed. The convective low and high-level loads affect the mixing and the exhaust node, respectively. The interface height determines if the vertical wall exchanges heat by convection with the floor air layer or the mixing node, and radiation from sources and surfaces is also included. Unlike Mateus's model, Lastovets's does not include recirculation flow patterns.

Kosonen et al. [40] compared the accuracy of Mundt's' 2-node, Arens' 2-node, Chen's 3-node, Nielsen's 2-node and Mateus's 3-node models in predicting the temperature distribution inside a simulated office room with different load combinations. They show that 2-node linear models generally underestimate the temperature in the occupied zone, where the heat sources are gathered. On the other hand, Mateus's 3-node model provides the best results, with an average error of 5.1 % among all the load configurations compared to measured data. However, the authors stress that its accuracy decreases when heat gains are located at a higher level, above the occupied zone. Similar outcomes are obtained by Lastovets et al. [131], who compared their 3-node model with Mundt's 2-node, Nielsen's 2-node, Mateus's 3-node and Rees's 9-node models. Their model overcomes Mateus's problems since it accurately predicts thermal stratification with higher heat gains, with an average error below 2 % for all experimental cases at the air nodes' height.

Lastovets et al. [135] constructed and validated a dynamic DV nodal model. It integrates the three-node DV model [131] into the room's resistance-capacitance (RC) network, as illustrated in Fig. 9. The building thermal mass is lumped into the parameter C_m, associated with floor, wall and ceiling structures. In addition, the heat capacity C_a is linked to the three air nodes, representing room air thermal inertia and furniture presence. These capacities and the thermal conductances constitute the model's parameters to be determined. The authors proposed a calibration process based on steady-state and dynamic set response parameter identification. The heat balance is set for each surface and air node under dynamic conditions, leading to a system of six differential equations to solve. Incorporating the system's thermal inertia, the model provides the transient evolution of the temperature gradient inside the space. The model has been applied to calculate the DV design airflow rate in a lecture room with different thermal masses and daily occupancy schedules [136].

Nodal models can be effectively employed in the temperature-based design of DV systems or integrated into building dynamic energy simulations. Currently, solar radiation is included only in Chen's [120] and Lastovets's [131,135] formulations, but both cases consider it as a direct heat load impinging on the air nodes; deeper modelling of incoming solar radiation and its distribution on internal surfaces should be considered in future developments. Moreover, heat sources of unequal strength generating multiple layers and mixing interfaces could be included. Despite their simplicity, these tools present a weak point: prior knowledge of the airflow patterns is needed, and generally, a pure vertical upward motion is assumed. Therefore, they are unsuitable for carrying out IAQ analysis with adequate accuracy.

On the other hand, zonal models can effectively predict both the airflow and temperature fields. The general modelling approach adopted for displacement ventilated rooms is shown in Fig. 10. Since DV operation produces a vertical stratification, the idea is to subdivide the space into horizontal layers, which in turn are discretized into zones or cells, representing portions of the room air volume. Heat sources' thermal plumes, updraft and downdraft regions along warm and cool walls are represented by special cells characterized by peculiar airflows, distinguishing them from the surrounding air. The airflow and temperature distributions are determined by solving each cell's mass and heat balances.

These tools have been conceived to carry out IAQ investigations concerning DV operation. Fig. 11 reports the main approaches adopted in literature works on the topic. Yamanaka et al. [137] assume a linear increase in pollutant concentration rather than a sharp variation across the stratification interface, where the plume and supply flow rate match. The space is subdivided into four layers, as

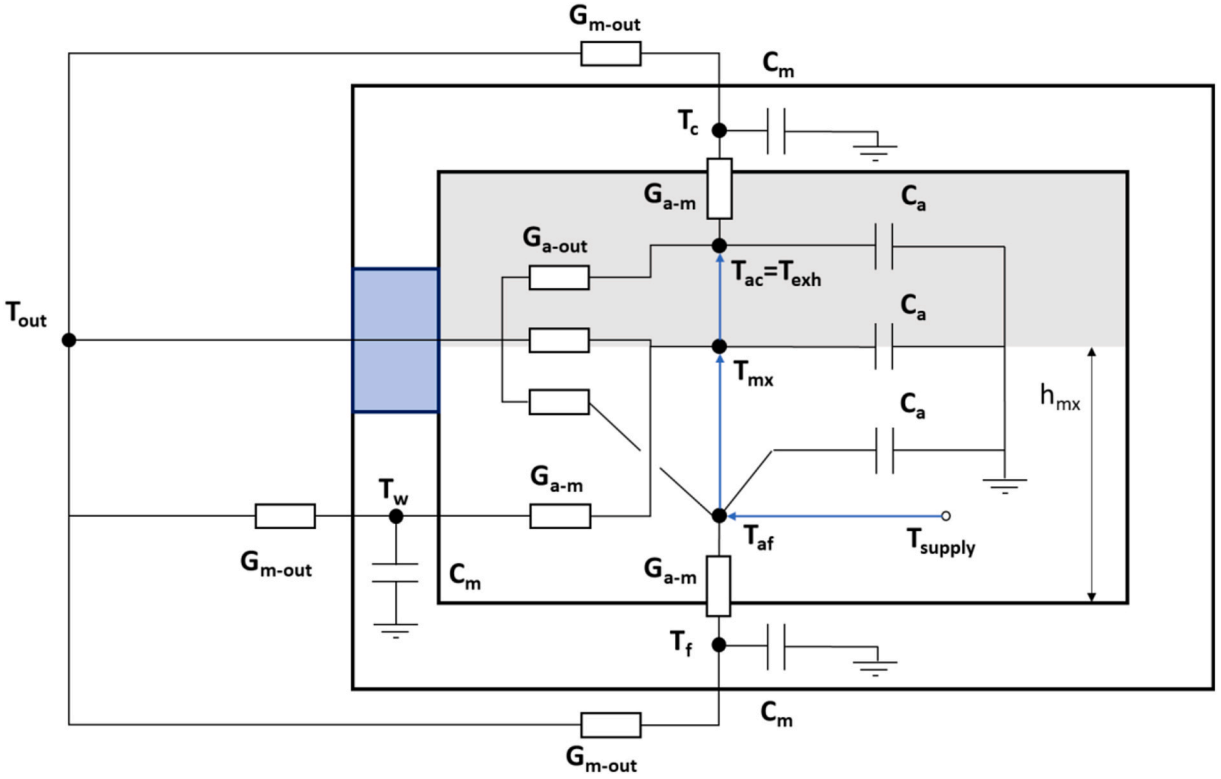

Fig. 9. Dynamic DV nodal model (Gi = thermal conductance) (adapted from Ref. [135]).

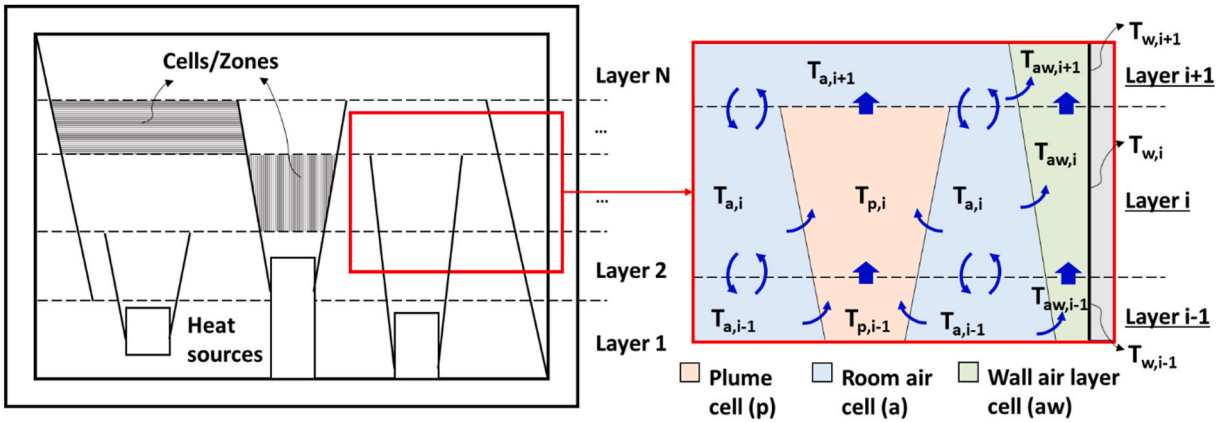

Fig. 10. Zonal modelling approach for displacement ventilated environments (Tw is the wall temperature in the layer; blue arrows represent the typical airflow patterns). (For interpretation of the references to colour in this figure legend, the reader is referred to the Web version of this article.)

shown in Fig. 11(a); the model includes the molecular and turbulent pollutant diffusion within the interface layer, air entrainment in the plumes and convective flows between the air layers. The concentration profile is obtained by solving the balance for each air layer. Choi et al. [41] proposed a five-layer model to account for the lock-up phenomenon, introducing the stagnation height with the concentration peak. Another work [76] enhances the four-layer model also to predict the temperature distribution, solving the heat balance for each layer. Both contaminant and heat diffusion occur inside the interface layer.

Fig. 11(b) presents the more rigorous approach employed by Habchi et al. [97]. It is a multi-plume, multi-layer transport model developed to study the distribution of active particles. The presence of non-interacting heat sources with unequal strength is considered. Three regions are identified in the vertical direction: Region I below the stratification interface where pollutants are emitted; Region II reaches the height where the buoyancy force of the strongest plume vanishes; Region III is the well-mixed ceiling layer. The model predicts temperature, airflow, and particle distribution by solving heat, mass, and concentration balances. Diffusion, gravitational settling and deposition rate on surfaces are also included since they significantly affect the spread of larger particles. The

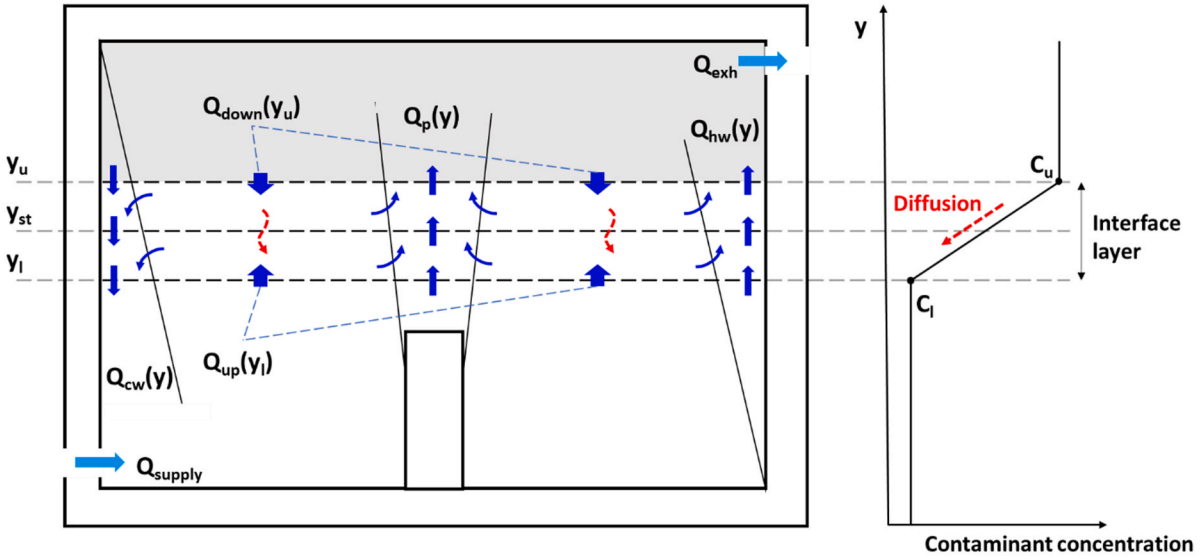

(a) Yamanaka's zonal model (adapted from [137])

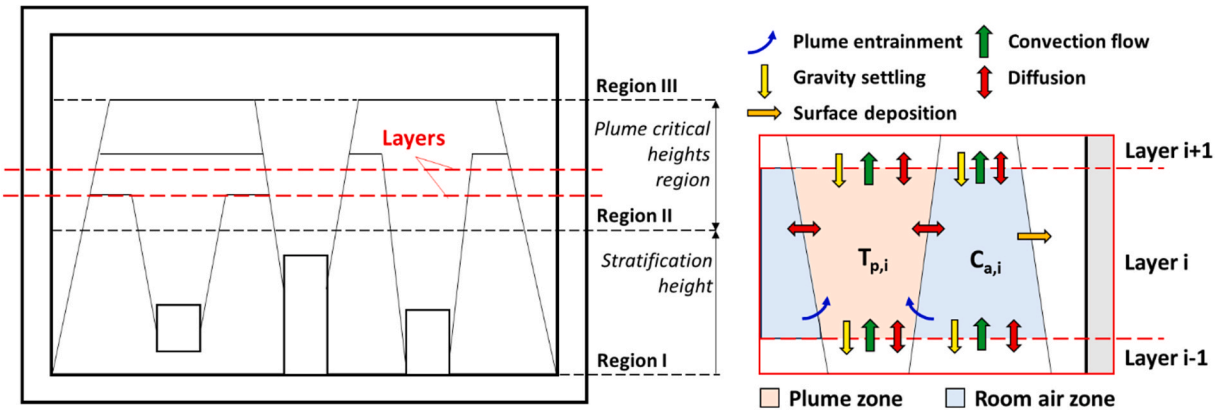

(b) Habchi's zonal model (adpated from [97])

Fig. 11. Adopted approaches in the analyses on IAQ with DV zonal models. (In Yamanaka's model figure: st=stratification height, u=upper edge, l=lower edge, hw=hot wall, cw=cold wall).

model has been upgraded to study cross-contamination between two occupants, incorporating the effect of the infected subject's exhalation jet from high-momentum respiratory activities, such as coughing or sneezing [138]. Two special cells are added: a cylindrical contaminated zone in front of the infected person where particles not entrained by the plume collect and the cylindrical exposure zone between the subjects.

Zonal models provide information on temperature, airflow and contaminant distribution with enough detail, so they are also appropriate for the IAQ-based design of DV systems. However, some aspects need to be faced in future research. The existing tools solve energy, mass and concentration balance under steady-state conditions, while the evolution of pollutant transport over time has not been examined yet. Moreover, the diffuser jet and the wake flows associated with occupants' movements should be incorporated together with thermal plumes, wall drafts and exhalation jets to include the effect of all airflow sources affecting the DV system performance.

4.3. Simplified methods for cooling load estimation

The working principle of displacement ventilation makes it suitable for space cooling rather than heating applications. Like other STRAD systems, DV focuses directly on the occupied zone, thus, only the cooling load in that region needs to be offset in the perspective of providing thermal comfort (Fig. 12(b)). The existing multi-zone building energy simulation tools assume perfect mixing, so all the convective heat released into the space contributes to the cooling load (Fig. 12(a)). The correct estimation of the cooling load in displacement ventilated spaces is essential when designing the system and evaluating its energy performance since it determines the required supply flow rate and the cooling coil load in the air handling system accordingly.

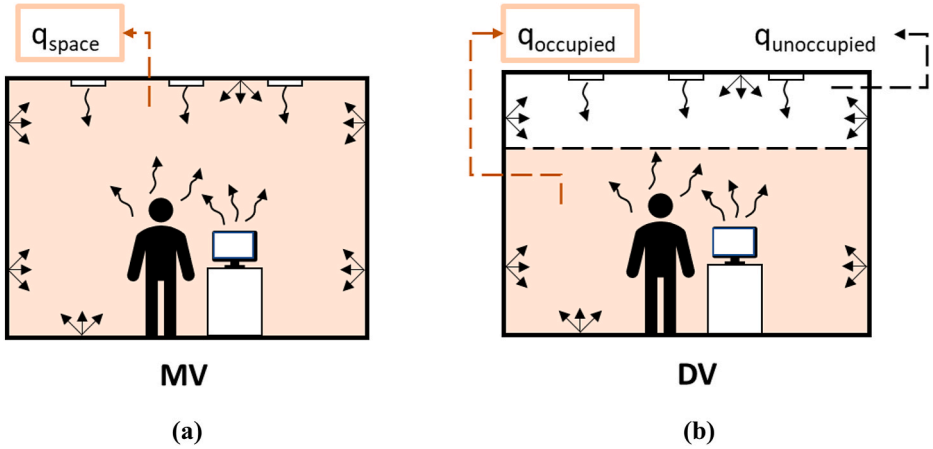

Fig. 12. Comparison of the cooling load calculation approaches between mixing (a) and displacement (b) ventilation. Black arrows represent the convective fluxes from heat sources and surfaces.

Some simplified methods for cooling load estimation have been proposed in different works. Two calculation approaches have been identified. In the first group, the basic idea is directly defining the load allocation to the occupied and unoccupied zone in relation to the position of the heat sources within the space. Xu et al. [105] express the contribution of each *i*-th heat source to the occupied zone load by defining the effective cooling load factor (ECLF) through Eq. (31).

$$ECLF_i = \frac{q_{i,occupied}}{q_{i,space}} \tag{31}$$

Both $q_{i,space}$ and $q_{i,occupied}$ are calculated for the individual heat source by assuming that the others are turned off. The former is the space cooling load in the case of perfect mixing and matches the source power. The latter is obtained from CFD simulations that provide the air enthalpy flux variation between the occupied zone's upper horizontal boundary and the supply vent. The total cooling load in the occupied zone is calculated by applying the superimposition of the effects.

$$q_{occupied} = \sum_{i\ source} \left(ECLF_i\ q_{i,space} \right) \tag{32}$$

The authors verified that neglecting the interactions due to the contemporary presence of multiple sources in defining the ECLF produces acceptable discrepancies on the computed $q_{occupied}$ compared to the real one. The cooling coil in the air handling unit (AHU) offsets the occupied zone load and the ventilation load, as expressed in Eq. (33).

$$q_{coil} = q_{occupied} + q_{vent} = \sum_{i\ source} \left(ECLF_i\ q_{i,space} \right) + Q_{out}\ \rho\ c_p\ (T_{out} - T_{set}) \tag{33}$$

Where Q_{out} is the outdoor air flow rate, and T_{set} is the setpoint temperature at head level. Cheng et al. [104] suggest that $q_{i,occupied}$ can also be calculated by summing the convective gain from the heat sources and the portion of surfaces in the occupied zone. The ECLF values for different heat sources and rooms can be found in Refs. [104,105,139]. Zhang et al. [140] incorporate indoor non-uniform temperature distributions into dynamic building energy simulations, introducing the contribution ratio of indoor climate (CRI). These factors represent the contribution of each *k*-th heat source to the temperature distribution and are defined through Eq. (34) as the ratio of temperature variation caused at a specific *j*-th location to that generated in the well-mixed scenario with the other sources inactivated.

$$CRI_{j,k} = \frac{\Delta T_{j,k}}{\Delta T_{well-mixed,k}} \tag{34}$$

The method is based on two main hypotheses. Firstly, a fixed airflow field is assumed, for which heat transfer linearity can be considered. Secondly, each heat source independently contributes to the temperature distribution, which results from the superimposition of individual subfields, as expressed by Eq. (35).

$$\Delta T_j = \sum_{k\ sources} \left(CRI_{j,k} \Delta T_{well-mixed,k} \right) \tag{35}$$

CFD modelling is employed to determine the representative airflow field and derive the CRI distribution for each source. The authors suggest that the energy simulation can be carried out by refining the zoning of the single room with reference to the heat sources' layout. The temperature of the subregion is calculated through Eq. (35) with average CRI. In their office case study, the thermal load calculated with the CRI method was 15–20 % lower than the perfect mixing-based energy simulation. The methodology is general for the STRAD systems, so its use can be broadened to DV, separating the occupied zone from the remainder. However, it requires the definition of multiple airflow field scenarios to be representative of as many heat load combinations as possible and to be

applicable to time-variant configurations. Similarly, Liang et al. [141] defined the average accessibility of the heat sources (AAHS) to correlate the local cooling load (LCL) to the heat gains in non-uniform thermal environments. The accessibility indexes express the influence of the individual heat sources on the average air temperature in a target region, e.g., the occupied zone. The local steady state value under a fixed airflow field is given by Eq. (36) for the *i*-th source.

$$AAHS_{zone,i} = \frac{T_{avg,zone,i} - T_{ref}}{\left(\frac{q_i}{Q_{supply}\ \rho\ c_p}\right)} \tag{36}$$

The average local temperature $T_{avg,\ zone,i}$ is determined through experimental tests or CFD simulations activating one source at a time. The target zone's desired setpoint can be considered the reference temperature T_{ref}. AAHS coefficients depend on airflow patterns, heat source distribution and size and location of the involved sub-volume. Once the indices are known for a given configuration, the local cooling load can be determined through Eq. (37):

$$q_{zone} = \sum_{i\ sources} \left(q_i\ AAHS_{zone,i}\right) \tag{37}$$

AAHS and CRI calculations are equivalent (Eqs. (36) and (34)), but the first method directly associates the accessibility factors with the local cooling load, while the latter defines the temperature distribution to be coupled with the building energy simulation tools. However, these methods based on the heat load breakdown present two drawbacks. Firstly, several CFD simulations must be carried out to provide a complete database of allocation parameters differentiated for types of heat sources and room configurations. In the second instance, the applicability of the superimposition of effects needs to be further investigated.

A second strategy proposes estimating the DV system's cooling load employing the existing building energy simulation tools, which are based on fully mixed air modelling and are computationally efficient. Zhang et al. [142] defined the equivalent room air temperature (ERAT) as the temperature assigned to the well-mixed building model to obtain the same cooling load in the DV case. The method can be applied to evaluate the energy performance of both constant-air-volume (CAV) and variable-air-volume (VAV) systems, for which the equivalent supply air temperature (ESAT) and the equivalent supply airflow rate (ESAR) are respectively defined as additional input parameters to the equivalent mixing ventilation system. The response surface methodology has been used to develop three data-driven models through polynomial regression: ERAT, ESAT and ESAR are expressed as functions of the actual room air temperature at 1.1 m, supply air temperature and flow rate. The authors proposed a calculation procedure to determine the DV system's cooling load and energy needs. For the CAV system, the building simulation tool is first fed with a first-guess ESAT and DV flow rate, and the ERAT is calculated. Secondly, the regression models are used to calculate the real supply conditions and the room air temperature. The ESAT is iteratively adjusted to maintain the desired setpoint for the latter. After comfort conditions are met, the actual cooling load is defined, and the exit air temperature is calculated accordingly. In this way, the energy needs in the air handling unit coils can be evaluated. The process is the same for the VAV system, with ESAR as an input parameter.

In contrast, Zhang et al. [143] identified the height in the displacement ventilated room for which the air temperature can be used as an input for the perfect mixing model to obtain an accurate estimation of the cooling load and the supply air temperature in a CAV system or the flow rate in a VAV system. They suggest that the height of the ceiling air layer can be employed and propose the corresponding procedure for the energy performance analyses involving the separate use of well-mixed air and multi-node models. The DV supply conditions are the input parameters for the well-mixed room model that calculates the cooling load and the room air temperature. In their formulation, this last parameter represents the exhaust air temperature. The nodal model is used to determine the temperature at 1.1 m, and supply conditions are iteratively adjusted to achieve thermal comfort. Afterwards, the required energy for air handling is estimated. The accuracy of these two methods in estimating the cooling load was verified by employing the output from the DV multi-node model as a benchmark for several validation case studies. Their advantage is directly incorporating the well-mixed model in the simulation process while considering the thermal stratification induced by the real DV system. However, the validity of system configurations that differ from those used for their development should be checked.

5. Conclusions

This paper reviewed the most significant literature dealing with displacement ventilation (DV). The temperature and airflow fields, as well as the contaminant transport, result from the complex interaction between the air distribution system and the enclosed space. A well-designed DV system supplying air at floor level generates a thermally stratified environment with a buoyancy-driven upward flow pushing the contaminant towards the ceiling for the extraction. The vertical temperature gradient and stratification height are strongly influenced by the heat sources' distribution and strength, the supply air conditions and the vents' location. The typical two-layer stratified space is obtained with heat gains located in the lower part of the room, and the interface height decreases at higher Archimedes numbers, expressing the ratio between the buoyancy and inertia forces. The steady-state airflow distribution is determined by the balance of different flow elements, i.e., diffuser jet, buoyant thermal plumes and their entrainment effect, recirculation from the upper mixed layer, and downdrafts along cool surfaces. The potential draft risk is generally avoided during DV operation since lower inlet velocity and turbulent fluctuations are observed compared to other ventilation systems. The stratified contaminant distribution presents a sharper interface than temperature, with an evident discontinuity between a clean occupied zone and a polluted ceiling layer. The air quality in the occupied zone depends on the types of pollutants and sources.

Compared to conventional mixing ventilation, displacement systems provide better indoor air quality at the same supply flow rate when active gaseous pollutant sources are present. Instead, the ventilation effectiveness in the occupied zone decreases if contaminant generation is not associated with a thermal plume or if the gravitational settlement of heavier particles dominates over the upward

flow. Moreover, DV performance is more sensitive to dynamic events, e.g., people movements, than MV since the recovery time of steady-state temperature, airflow and contaminant distributions is much longer. Regarding cooling energy demand, DV has more saving potential than MV since a lower supply flow rate and higher supply temperature are required for the same IAQ and thermal comfort level in the occupied zone.

Different simplified modelling approaches can be employed in building energy simulations to evaluate DV performance and to aid the design and control of the system. Analytical models are based on the plume theory and can be employed to calculate the design flow rate, but they are unsuitable for energy and comfort evaluation. The applicability of empirical correlations is restricted to a particular system's configuration, and their generalization is difficult. Nodal models accurately predict the vertical temperature profile and are easy to integrate into building energy simulation tools; however, they require prior knowledge of the airflow patterns in the room. Zonal models can be employed to define temperature and airflow distributions, even if few studies have applied them. Simplified methods for cooling load estimation have also been developed to study system performance while modelling the building using classical well-mixing tools. Moreover, correctly calculating the cooling load in the occupied zone leads to a more accurate DV design, avoiding oversized systems.

The desk research highlighted that DV has been widely studied, and its working principles are well understood now. The current research activity is proceeding on HVAC systems integrating DV to radiant panels since the latter are widely installed in new energy-efficient or retrofitted buildings; deeper analyses of the fluid dynamic of different combinations are needed to establish clear design guidelines of the coupled systems, even for different configurations from typical DV/CC. Nevertheless, some points need to be investigated even more in the future. More attention must be given to DV's effectiveness in removing heavier contaminants, especially in the context of airborne transmission of respiratory diseases. Moreover, it is observed that not many works deal with the energy aspects yet. For example, some authors roughly estimate the DV energy performance in studies where the main objective is defining how the thermal environment or IAQ are affected. More in-depth analyses combining energy efficiency and cost-effectiveness assessments would be interesting and necessary to determine DV systems' overall energy and economic impact. The assessment of DV operation under dynamic conditions should be promoted toward optimal system design and control. Given DV's sensitivity to transient disturbances, it would be interesting to analyse how the system could be dynamically adjusted in response to changing heat load configurations and the influence of incoming solar radiation, which typically affects commercial buildings' indoor spaces. The research has not yet taken on these aspects in detail. Dynamic RC multi-node models could be improved in parallel to integrate the impact of solar radiation and its distribution on internal surfaces. In this way, the space dynamic behaviour under the operation of the DV system would be adequately assessed.

CRediT authorship contribution statement

Giacomo Tognon: Writing – original draft, Visualization, Methodology, Investigation, Conceptualization. **Angelo Zarrella:** Writing – review & editing, Visualization, Supervision, Conceptualization.

Declaration of competing interest

The authors declare that they have no known competing financial interests or personal relationships that could have appeared to influence the work reported in this paper.

Data availability

No data was used for the research described in the article.

References

[1] Eurostat, Energy Data, 2020 edition, 2020, https://doi.org/10.2785/68334.
[2] European Commission, Energy Roadmap 2050 Impact Assessment and Scenario Analysis, 2011. Brussels.
[3] Y. Geng, W. Ji, B. Lin, Y. Zhu, The impact of thermal environment on occupant IEQ perception and productivity, Build. Environ. 121 (2017) 158–167, https://doi.org/10.1016/j.buildenv.2017.05.022.
[4] S.B. Sadineni, S. Madala, R.F. Boehm, Passive building energy savings: a review of building envelope components, Renew. Sustain. Energy Rev. 15 (2011) 3617–3631, https://doi.org/10.1016/j.rser.2011.07.014.
[5] L. Zaniboni, R. Albatici, Natural and mechanical ventilation concepts for indoor comfort and well-being with a sustainable design perspective: a systematic review, Buildings 12 (2022), https://doi.org/10.3390/buildings12111983.
[6] M. Fan, Z. Fu, J. Wang, Z. Wang, H. Suo, X. Kong, H. Li, A review of different ventilation modes on thermal comfort, air quality and virus spread control, Build. Environ. 212 (2022), https://doi.org/10.1016/j.buildenv.2022.108831.
[7] E. Mesenhöller, P. Vennemann, J. Hussong, Unsteady room ventilation – a review, Build. Environ. 169 (2020), https://doi.org/10.1016/j.buildenv.2019.106595.
[8] C. Buonocore, R. De Vecchi, R. Lamberts, S. Güths, From characterisation to evaluation: a review of dynamic and non-uniform airflows in thermal comfort studies, Build. Environ. 206 (2021), https://doi.org/10.1016/j.buildenv.2021.108386.
[9] B. Yang, A.K. Melikov, A. Kabanshi, C. Zhang, F.S. Bauman, G. Cao, H. Awbi, H. Wigö, J. Niu, K.W.D. Cheong, K.W. Tham, M. Sandberg, P.V. Nielsen, R. Kosonen, R. Yao, S. Kato, S.C. Sekhar, S. Schiavon, T. Karimipanah, X. Li, Z. Lin, A review of advanced air distribution methods - theory, practice, limitations and solutions, Energy Build. 202 (2019), https://doi.org/10.1016/j.enbuild.2019.109359.
[10] G. Cao, H. Awbi, R. Yao, Y. Fan, K. Sirén, R. Kosonen, J Jensen Zhang, A review of the performance of different ventilation and airflow distribution systems in buildings, Build. Environ. 73 (2014) 171–186, https://doi.org/10.1016/j.buildenv.2013.12.009.
[11] B.W. Olesen, M. Schøler, P.O. Fanger, Discomfort caused by vertical air temperature differences, in: P.O. Fanger, 0 Valbjorn (Eds.), Indoor Climate: Effects on Human Comfort, Performance and Health in Residential, Commercial and Light-Industry Buildings, Danish Building Research Institute, Copenhagen, Denmark, 1979.

[12] S. Liu, Z. Wang, S. Schiavon, Y. He, M. Luo, H. Zhang, E. Arens, Predicted percentage dissatisfied with vertical temperature gradient, Energy Build. 220 (2020), https://doi.org/10.1016/j.enbuild.2020.110085.
[13] ASHRAE, ANSI/ASHRAE standard 55-2017: thermal environmental conditions for human occupancy. www.ashrae.org/technology, 2017.
[14] E.C. for Standardization, EN ISO 7730:2005 - Ergonomics of the Thermal Environment-Analytical Determination and Interpretation of Thermal Comfort Using Calculation of the PMV and PPD Indices and Local Thermal Comfort Criteria, 2005.
[15] X. Yuan, Q. Chen, L.R. Glicksman, A critical review of displacement ventilation, Build. Eng. 104 (1998) 78–90.
[16] H. Skistad, E. Mundt, P. V Nielsen, K. Hagström, J. Railio, Displacement Ventilation in Non-industrial Premises, REHVA, 2002.
[17] X. Yuan, Q. Chen, L.R. Glicksman, Performance evaluation and design guidelines for displacement ventilation, Build. Eng. 105 (1999).
[18] Q. Chen, L. Glicksman, System Performance Evaluation and Design Guidelines for Displacement Ventilation, ASHRAE, 2003. www.ashrae.org.
[19] A.M. Elsaid, H.A. Mohamed, G.B. Abdelaziz, M.S. Ahmed, A critical review of heating, ventilation, and air conditioning (HVAC) systems within the context of a global SARS-CoV-2 epidemic, Process Saf. Environ. Protect. 155 (2021) 230–261, https://doi.org/10.1016/j.psep.2021.09.021.
[20] W. Zheng, J. Hu, Z. Wang, J. Li, Z. Fu, H. Li, J. Jurasz, S.K. Chou, J. Yan, COVID-19 impact on operation and energy consumption of heating, ventilation and air-conditioning (HVAC) systems, Advances in Applied Energy 3 (2021), https://doi.org/10.1016/j.adapen.2021.100040.
[21] P. Carrer, P. Wargocki, A. Fanetti, W. Bischof, E. De Oliveira Fernandes, T. Hartmann, S. Kephalopoulos, S. Palkonen, O. Seppänen, What does the scientific literature tell us about the ventilation-health relationship in public and residential buildings? Build. Environ. 94 (2015) 273–286, https://doi.org/10.1016/j.buildenv.2015.08.011.
[22] L. Morawska, J.W. Tang, W. Bahnfleth, P.M. Bluyssen, A. Boerstra, G. Buonanno, J. Cao, S. Dancer, A. Floto, F. Franchimon, C. Haworth, J. Hogeling, C. Isaxon, J.L. Jimenez, J. Kurnitski, Y. Li, M. Loomans, G. Marks, L.C. Marr, L. Mazzarella, A.K. Melikov, S. Miller, D.K. Milton, W. Nazaroff, P.V. Nielsen, C. Noakes, J. Peccia, X. Querol, C. Sekhar, O. Seppänen, S. ichi Tanabe, R. Tellier, K.W. Tham, P. Wargocki, A. Wierzbicka, M. Yao, How can airborne transmission of COVID-19 indoors be minimised? Environ. Int. 142 (2020) https://doi.org/10.1016/j.envint.2020.105832.
[23] Z. Noorimotlagh, N. Jaafarzadeh, S.S. Martínez, S.A. Mirzaee, A systematic review of possible airborne transmission of the COVID-19 virus (SARS-CoV-2) in the indoor air environment, Environ. Res. 193 (2021), https://doi.org/10.1016/j.envres.2020.110612.
[24] G. Berry, A. Parsons, M. Morgan, J. Rickert, H. Cho, A review of methods to reduce the probability of the airborne spread of COVID-19 in ventilation systems and enclosed spaces, Environ. Res. 203 (2022), https://doi.org/10.1016/j.envres.2021.111765.
[25] R.K. Bhagat, P.F. Linden, Displacement ventilation: a viable ventilation strategy for makeshift hospitals and public buildings to contain COVID-19 and other airborne diseases: ventilation strategy for COVID-19, R. Soc. Open Sci. 7 (2020), https://doi.org/10.1098/rsos.200680.
[26] Q. Chen, Can we migrate COVID-19 spreading risk? Front. Environ. Sci. Eng. 15 (2021) https://doi.org/10.1007/s11783-020-1328-8.
[27] ScienceDirect, (n.d.). https://www.sciencedirect.com/(accessed January 5, 2024).
[28] Web of Science, (n.d.). https://access.clarivate.com/login?app=wos&alternative=true&shibShireURL=https:%2F%2Fwww.webofknowledge.com%2F%3Fauth%3DShibboleth&shibReturnURL=https:%2F%2Fwww.webofknowledge.com%2F%3FDestApp%3DUA%26action%3Dtransfer%26mode%3DNextgen%26path%3D%252Fwos%252Fwoscc%252Fbasic-search&referrer=mode%3DNextgen%26path%3D%252Fwos%252Fwoscc%252Fbasic-search%26DestApp%3DUA%26action%3Dtransfer&roaming=true (accessed January 5, 2024).
[29] X. Yuan, Q. Chen, L.R. Glicksman, Y. Hu, X. Yang, Measurements and computations of room airflow with displacement ventilation, Build. Eng. 105 (1999).
[30] P.F. Linden, G.F. Lane-Serff, D.A. Smeed, Emptying filling boxes : the fluid mechanics of natural ventilation, J. Fluid Mech. (1990) 309–335.
[31] N. Mingotti, A.W. Woods, On the transport of heavy particles through an upward displacement-ventilated space, J. Fluid Mech. 772 (2015) 478–507, https://doi.org/10.1017/jfm.2015.204.
[32] S. Gilani, H. Montazeri, B. Blocken, CFD simulation of stratified indoor environment in displacement ventilation: validation and sensitivity analysis, Build. Environ. 95 (2016) 299–313, https://doi.org/10.1016/j.buildenv.2015.09.010.
[33] J. Taghinia, M.M. Rahman, T. Siikonen, Numerical simulation of airflow and temperature fields around an occupant in indoor environment, Energy Build. 104 (2015) 199–207, https://doi.org/10.1016/j.enbuild.2015.06.085.
[34] M. Jin, W. Liu, Q. Chen, Simulating buoyancy-driven airflow in buildings by coarse-grid fast fluid dynamics, Build. Environ. 85 (2015) 144–152, https://doi.org/10.1016/j.buildenv.2014.11.028.
[35] B. Liu, K. Min, J. Song, Effect of thermal plume on personal thermal comfort in displacement ventilation at one side of the room, in: Procedia Eng, Elsevier Ltd, 2015, pp. 1058–1066, https://doi.org/10.1016/j.proeng.2015.09.103.
[36] X. Tian, B. Li, Y. Ma, D. Liu, Y. Li, Y. Cheng, Experimental study of local thermal comfort and ventilation performance for mixing, displacement and stratum ventilation in an office, Sustain. Cities Soc. 50 (2019), https://doi.org/10.1016/j.scs.2019.101630.
[37] H. Chen, S. Janbakhsh, U. Larsson, B. Moshfegh, Numerical investigation of ventilation performance of different air supply devices in an office environment, Build. Environ. 90 (2015) 37–50, https://doi.org/10.1016/j.buildenv.2015.03.021.
[38] A.K. Melikov, Human body micro-environment: the benefits of controlling airflow interaction, Build. Environ. 91 (2015) 70–77, https://doi.org/10.1016/j.buildenv.2015.04.010.
[39] P. V Nielsen, Vertical temperature distribution in a room with displacement ventilation, dept. Of building technology and structural engineering, Indoor Environmental Technology R9509 (48) (1995) 9509.
[40] R. Kosonen, N. Lastovets, P. Mustakallio, G.C. da Graça, N.M. Mateus, M. Rosenqvist, The effect of typical buoyant flow elements and heat load combinations on room air temperature profile with displacement ventilation, Build. Environ. 108 (2016) 207–219, https://doi.org/10.1016/j.buildenv.2016.08.037.
[41] N. Choi, T. Yamanaka, K. Sagara, Y. Momoi, T. Suzuki, Displacement ventilation with radiant panel for hospital wards: measurement and prediction of the temperature and contaminant concentration profiles, Build. Environ. 160 (2019), https://doi.org/10.1016/j.buildenv.2019.106197.
[42] X. Yang, K. Zhong, Y. Kang, T. Tao, Numerical investigation on the airflow characteristics and thermal comfort in buoyancy-driven natural ventilation rooms, Energy Build. 109 (2015) 255–266, https://doi.org/10.1016/j.enbuild.2015.09.071.
[43] Y. Wang, F.Y. Zhao, J. Kuckelkorn, D. Liu, J. Liu, J.L. Zhang, Classroom energy efficiency and air environment with displacement natural ventilation in a passive public school building, Energy Build. 70 (2014) 258–270, https://doi.org/10.1016/j.enbuild.2013.11.071.
[44] F.A. Dominguez Espinosa, L.R. Glicksman, Determining thermal stratification in rooms with high supply momentum, Build. Environ. 112 (2017) 99–114, https://doi.org/10.1016/j.buildenv.2016.11.016.
[45] M.L. Fong, V. Hanby, R. Greenough, Z. Lin, Y. Cheng, Acceptance of thermal conditions and energy use of three ventilation strategies with six exhaust configurations for the classroom, Build. Environ. 94 (2015) 606–619, https://doi.org/10.1016/j.buildenv.2015.10.024.
[46] Y. Cheng, Z. Lin, Experimental study of airflow characteristics of stratum ventilation in a multi-occupant room with comparison to mixing ventilation and displacement ventilation, Indoor Air 25 (2015) 662–671, https://doi.org/10.1111/ina.12188.
[47] Y.J.P. Lin, C.L. Lin, A study on flow stratification in a space using displacement ventilation, Int. J. Heat Mass Tran. 73 (2014) 67–75, https://doi.org/10.1016/j.ijheatmasstransfer.2014.01.067.
[48] Y. Wang, F.Y. Zhao, J. Kuckelkorn, H. Spliethoff, E. Rank, School building energy performance and classroom air environment implemented with the heat recovery heat pump and displacement ventilation system, Appl. Energy 114 (2014) 58–68, https://doi.org/10.1016/j.apenergy.2013.09.020.
[49] Y.J.P. Lin, J.Y. Wu, A study on density stratification by mechanical extraction displacement ventilation, Int. J. Heat Mass Tran. 110 (2017) 447–459, https://doi.org/10.1016/j.ijheatmasstransfer.2017.03.053.
[50] Z. Liu, S. Cai, S. Li, Experimental research on the temperature distribution of natural displacement ventilation in the room under the influence of wind pressure and air supply, in: Procedia Eng, Elsevier Ltd, 2017, pp. 989–995, https://doi.org/10.1016/j.proeng.2017.10.156.
[51] R. Yang, C.S. Ng, K.L. Chong, R. Verzicco, D. Lohse, Do increased flow rates in displacement ventilation always lead to better results? J. Fluid Mech. 932 (2022) https://doi.org/10.1017/jfm.2021.949.
[52] A.Q. Ahmed, S. Gao, A.K. Kareem, A numerical study on the effects of exhaust locations on energy consumption and thermal environment in an office room served by displacement ventilation, Energy Convers. Manag. 117 (2016) 74–85, https://doi.org/10.1016/j.enconman.2016.03.004.

[53] T. Gil-Lopez, M.A. Galvez-Huerta, P.G. O'Donohoe, J. Castejon-Navas, P.M. Dieguez-Elizondo, Analysis of the influence of the return position in the vertical temperature gradient in displacement ventilation systems for large halls, Energy Build. 140 (2017) 371–379, https://doi.org/10.1016/j.enbuild.2017.02.017.
[54] Y. Cheng, J. Niu, X. Liu, N. Gao, Experimental and numerical investigations on stratified air distribution systems with special configuration: thermal comfort and energy saving, Energy Build. 64 (2013) 154–161, https://doi.org/10.1016/j.enbuild.2013.04.026.
[55] M.A. Menchaca-Brandan, F.A. Dominguez Espinosa, L.R. Glicksman, The influence of radiation heat transfer on the prediction of air flows in rooms under natural ventilation, Energy Build. 138 (2017) 530–538, https://doi.org/10.1016/j.enbuild.2016.12.037.
[56] J. Le Dréau, P. Heiselberg, R.L. Jensen, Experimental investigation of convective heat transfer during night cooling with different ventilation systems and surface emissivities, Energy Build. 61 (2013) 308–317, https://doi.org/10.1016/j.enbuild.2013.02.021.
[57] W. Wu, Z. Lin, An experimental study of the influence of a walking occupant on three air distribution methods, Build. Environ. 85 (2015) 211–219, https://doi.org/10.1016/j.buildenv.2014.12.009.
[58] W. Wu, Z. Lin, Experimental study of the influence of a moving manikin on temperature profile and carbon dioxide distribution under three air distribution methods, Build. Environ. 87 (2015) 142–153, https://doi.org/10.1016/j.buildenv.2015.01.027.
[59] L. Feng, F. Zeng, R. Li, R. Ju, N. Gao, Influence of manikin movement on temperature stratification in a displacement ventilated room, Energy Build. 234 (2021), https://doi.org/10.1016/j.enbuild.2020.110700.
[60] C. Zhang, M. Pomianowski, P.K. Heiselberg, T. Yu, A review of integrated radiant heating/cooling with ventilation systems- Thermal comfort and indoor air quality, Energy Build. 223 (2020), https://doi.org/10.1016/j.enbuild.2020.110094.
[61] A. Novoselac, J. Srebric, A critical review on the performance and design of combined cooled ceiling and displacement ventilation systems, Energy Build. 34 (2002) 497–509.
[62] W. Shan, D. Rim, Thermal and ventilation performance of combined passive chilled beam and displacement ventilation systems, Energy Build. 158 (2018) 466–475, https://doi.org/10.1016/j.enbuild.2017.10.010.
[63] Z. Shi, Z. Lu, Q. Chen, Indoor airflow and contaminant transport in a room with coupled displacement ventilation and passive-chilled-beam systems, Build. Environ. 161 (2019), https://doi.org/10.1016/j.buildenv.2019.106244.
[64] Z. Shi, D. Lai, Q. Chen, Performance evaluation and design guide for a coupled displacement-ventilation and passive-chilled-beam system, Energy Build. 208 (2020), https://doi.org/10.1016/j.enbuild.2019.109654.
[65] S.J. Rees, P. Haves, An experimental study of air flow and temperature distribution in a room with displacement ventilation and a chilled ceiling, Build. Environ. 59 (2013) 358–368, https://doi.org/10.1016/j.buildenv.2012.09.001.
[66] Y. Yang, Y. Wang, X. Yuan, Y. Zhu, D. Zhang, Simulation study on the thermal environment in an office with radiant cooling and displacement ventilation system, in: Procedia Eng, Elsevier Ltd, 2017, pp. 3146–3153, https://doi.org/10.1016/j.proeng.2017.10.142.
[67] M. Krajčík, R. Tomasi, A. Simone, B.W. Olesen, Experimental study including subjective evaluations of mixing and displacement ventilation combined with radiant floor heating/cooling system, HVAC R Res. 19 (2013) 1063–1072, https://doi.org/10.1080/10789669.2013.806173.
[68] M. Krajčík, R. Tomasi, A. Simone, B.W. Olesen, Thermal comfort and ventilation effectiveness in an office room with radiant floor cooling and displacement ventilation, Sci Technol Built Environ 22 (2016) 317–327, https://doi.org/10.1080/23744731.2016.1131568.
[69] X. Wu, L. Fang, B.W. Olesen, J. Zhao, F. Wang, Air distribution in a multi-occupant room with mixing or displacement ventilation with or without floor or ceiling heating, Sci Technol Built Environ 21 (2015) 1109–1116, https://doi.org/10.1080/23744731.2015.1090255.
[70] X. Wu, J. Gao, H. Wang, L. Fang, B.W. Olesen, Indoor thermal environment and air distribution in a floor-ceiling heating room with mixing or displacement ventilation, Sci Technol Built Environ 25 (2019) 346–355, https://doi.org/10.1080/23744731.2018.1527138.
[71] T.B. Moodie, Gravity currents, J. Comput. Appl. Math. 144 (2002) 49–83. www.elsevier.com/locate/cam.
[72] L. Magnier-Bergeron, D. Derome, R. Zmeureanu, Three-dimensional model of air speed in the secondary zone of displacement ventilation jet, Build. Environ. 114 (2017) 483–494, https://doi.org/10.1016/j.buildenv.2017.01.003.
[73] R. Li, C. Huang, X. Gao, X. Wang, A study of the temperature characteristics of low speed curved surface jet in the lower air supply area, in: Procedia Eng, Elsevier Ltd, 2017, pp. 2553–2560, https://doi.org/10.1016/j.proeng.2017.10.231.
[74] I. Fatemi, B.C. Wang, M. Koupriyanov, B. Tully, Experimental study of a non-isothermal wall jet issued by a displacement ventilation system, Build. Environ. 66 (2013) 131–140, https://doi.org/10.1016/j.buildenv.2013.04.019.
[75] A. Fernández-Gutiérrez, I. González-Prieto, L. Parras, P. Gutiérrez-Castillo, J.M. Cejudo-López, C. Del Pino, Experimental and numerical study of a small-scale and low-velocity indoor diffuser for displacement ventilation: isothermal floor, Appl. Therm. Eng. 87 (2015) 79–88, https://doi.org/10.1016/j.applthermaleng.2014.12.078.
[76] N. Choi, T. Yamanaka, T. Kobayashi, T. Ihama, M. Wakasa, Influence of vertical airflow along walls on temperature and contaminant concentration distributions in a displacement-ventilated four-bed hospital ward, Build. Environ. 183 (2020), https://doi.org/10.1016/j.buildenv.2020.107181.
[77] Z. Cheng, C. Guangyu, A. Aganovic, L. Baizhan, Experimental study of the interaction between thermal plumes and human breathing in an undisturbed indoor environment, Energy Build. 207 (2020), https://doi.org/10.1016/j.enbuild.2019.109587.
[78] Y. Wu, N. Gao, The dynamics of the body motion induced wake flow and its effects on the contaminant dispersion, Build. Environ. 82 (2014) 63–74, https://doi.org/10.1016/j.buildenv.2014.08.003.
[79] J. Liu, Z. Lin, Energy and exergy analyze of different air distributions in a residential building, Energy Build. 233 (2021), https://doi.org/10.1016/j.enbuild.2020.110694.
[80] W. Zhao, S. Lestinen, P. Mustakallio, S. Kilpeläinen, J. Jokisalo, R. Kosonen, Experimental study on thermal environment in a simulated classroom with different air distribution methods, J. Build. Eng. 43 (2021), https://doi.org/10.1016/j.jobe.2021.103025.
[81] S. Schiavon, D. Rim, W. Pasut, W.W. Nazaroff, Sensation of draft at uncovered ankles for women exposed to displacement ventilation and underfloor air distribution systems, Build. Environ. 96 (2016) 228–236, https://doi.org/10.1016/j.buildenv.2015.11.009.
[82] H. Ahn, D. Rim, L.J. Lo, Ventilation and energy performance of partitioned indoor spaces under mixing and displacement ventilation, Build. Simulat. 11 (2018) 561–574, https://doi.org/10.1007/s12273-017-0410-z.
[83] S. Liu, M. Koupriyanov, D. Paskaruk, G. Fediuk, Q. Chen, Investigation of airborne particle exposure in an office with mixing and displacement ventilation, Sustain. Cities Soc. 79 (2022), https://doi.org/10.1016/j.scs.2022.103718.
[84] X. Tian, S. Zhang, H.B. Awbi, C. Liao, Y. Cheng, Z. Lin, Multi-indicator evaluation on ventilation effectiveness of three ventilation methods: an experimental study, Build. Environ. 180 (2020), https://doi.org/10.1016/j.buildenv.2020.107015.
[85] D.R. Irwin, C.J. Simonson, K.Y. Saw, R.W. Besant, Contaminant and heat removal effectiveness and air-to-air heat/energy recovery for a contaminated air space, Build. Eng. 104 (1998).
[86] Z. Shi, Q. Chen, Experimental and computational investigation of wall-mounted displacement induction ventilation system, Energy Build. 241 (2021), https://doi.org/10.1016/j.enbuild.2021.110937.
[87] A. Jurelionis, L. Gagyte, T. Prasauskas, D. Čiužas, E. Krugly, L. Šeduikyte, D. Martuzevičius, The impact of the air distribution method in ventilated rooms on the aerosol particle dispersion and removal: the experimental approach, Energy Build. 86 (2015) 305–313, https://doi.org/10.1016/j.enbuild.2014.10.014.
[88] F.A. Berlanga, M.R. de Adana, I. Olmedo, J.M. Villafruela, J.F. San José, F. Castro, Experimental evaluation of thermal comfort, ventilation performance indices and exposure to airborne contaminant in an airborne infection isolation room equipped with a displacement air distribution system, Energy Build. 158 (2018) 209–221, https://doi.org/10.1016/j.enbuild.2017.09.100.
[89] S.R. Ardkapan, P.V. Nielsen, A. Afshari, Studying passive ultrafine particle dispersion in a room with a heat source, Build. Environ. 71 (2014) 1–6, https://doi.org/10.1016/j.buildenv.2013.09.012.
[90] Y.E. Cetin, M. Avci, O. Aydin, Particle dispersion and deposition in displacement ventilation systems combined with floor heating, Sci Technol Built Environ 26 (2020) 1019–1036, https://doi.org/10.1080/23744731.2020.1760637.
[91] S. Alotaibi, W. Chakroun, C. Habchi, K. Ghali, N. Ghaddar, Influence of mixed and displacement air distribution systems' design on concentrations of micro-particles emitted from floor or generated by breathing, J. Build. Eng. 26 (2019), https://doi.org/10.1016/j.jobe.2019.100855.

[92] P. Carlotti, B. Massoulié, A. Morez, A. Villaret, L. Jing, T. Vrignaud, A. Pfister, Respiratory pandemic and indoor aeraulics of classrooms, Build. Environ. 212 (2022), https://doi.org/10.1016/j.buildenv.2022.108756.
[93] J. Wang, J. Yang, J. Yu, F. Xiong, Comparative characteristics of relative pollution exposure caused by human surface chemical reaction under mixing and displacement ventilation, Build. Environ. 132 (2018) 225–232, https://doi.org/10.1016/j.buildenv.2018.01.044.
[94] G. Pei, D. Rim, S. Schiavon, M. Vannucci, Effect of sensor position on the performance of CO2-based demand controlled ventilation, Energy Build. 202 (2019), https://doi.org/10.1016/j.enbuild.2019.109358.
[95] Q. Zhou, H. Qian, H. Ren, Y. Li, P.V. Nielsen, The lock-up phenomenon of exhaled flow in a stable thermally-stratified indoor environment, Build. Environ. 116 (2017) 246–256, https://doi.org/10.1016/j.buildenv.2017.02.010.
[96] N.M. Mateus, G. Carrilho da Graça, Simulated and measured performance of displacement ventilation systems in large rooms, Build. Environ. 114 (2017) 470–482, https://doi.org/10.1016/j.buildenv.2017.01.002.
[97] C. Habchi, K. Ghali, N. Ghaddar, A simplified mathematical model for predicting cross contamination in displacement ventilation air-conditioned spaces, J. Aerosol Sci. 76 (2014) 72–86, https://doi.org/10.1016/j.jaerosci.2014.05.009.
[98] G. Brockmann, M. Kriegel, Airborne infection prevention: a comparisson of mixing ventilation and displacement ventilation in a meeting room. https://doi.org/10.14279/depositonce-10421, 2020.
[99] W. Su, B. Yang, A. Melikov, C. Liang, Y. Lu, F. Wang, A. Li, Z. Lin, X. Li, G. Cao, R. Kosonen, Infection probability under different air distribution patterns, Build. Environ. 207 (2022), https://doi.org/10.1016/j.buildenv.2021.108555.
[100] J.M. Villafruela, I. Olmedo, J.F. San José, Influence of human breathing modes on airborne cross infection risk, Build. Environ. 106 (2016) 340–351, https://doi.org/10.1016/j.buildenv.2016.07.005.
[101] B.P.P. Barbosa, N. de Carvalho Lobo Brum, Ventilation mode performance against airborne respiratory infections in small office spaces: limits and rational improvements for Covid-19, J. Braz. Soc. Mech. Sci. Eng. 43 (2021), https://doi.org/10.1007/s40430-021-03029-x.
[102] J. Shen, M. Kong, B. Dong, M.J. Birnkrant, J. Zhang, A systematic approach to estimating the effectiveness of multi-scale IAQ strategies for reducing the risk of airborne infection of SARS-CoV-2, Build. Environ. 200 (2021), https://doi.org/10.1016/j.buildenv.2021.107926.
[103] J. Huang, T. Hao, X. Liu, P. Jones, C. Ou, W. Liang, F. Liu, Airborne transmission of the Delta variant of SARS-CoV-2 in an auditorium, Build. Environ. 219 (2022), https://doi.org/10.1016/j.buildenv.2022.109212.
[104] Y. Cheng, J. Niu, N. Gao, Stratified air distribution systems in a large lecture theatre: a numerical method to optimize thermal comfort and maximize energy saving, Energy Build. 55 (2012) 515–525, https://doi.org/10.1016/j.enbuild.2012.09.021.
[105] H. Xu, N. Gao, J. Niu, A method to generate effective cooling load factors for stratified air distribution systems using a floor-level air supply, HVAC R Res. 15 (2009) 915–930, https://doi.org/10.1080/10789669.2009.10390872.
[106] M.L. Fong, Z. Lin, K.F. Fong, V. Hanby, R. Greenough, Life cycle assessment for three ventilation methods, Build. Environ. 116 (2017) 73–88, https://doi.org/10.1016/j.buildenv.2017.02.006.
[107] X. Wang, Z. Lin, An experimental investigation into the pull-down performances with different air distributions, Appl. Therm. Eng. 91 (2015) 151–162, https://doi.org/10.1016/j.applthermaleng.2015.08.012.
[108] S.A. Klein, et al., Trnsys 18: a transient system simulation program, Madison, USA, http://sel.me.wisc.edu/trnsys, 2017.
[109] EnergyPlusTM version 22.1, 0 Documentation Engineering Reference, 2022.
[110] W. Tian, X. Han, W. Zuo, M.D. Sohn, Building energy simulation coupled with CFD for indoor environment: a critical review and recent applications, Energy Build. 165 (2018) 184–199, https://doi.org/10.1016/j.enbuild.2018.01.046.
[111] Y.J.P. Lin, Y.C. Fan, Study on emptying-box problem with different inflow directions, Int. J. Heat Mass Tran. 92 (2016) 1009–1017, https://doi.org/10.1016/j.ijheatmasstransfer.2015.09.038.
[112] B.R. Morton, G. Taylor, J.S. Turner, Turbulent gravitational convection from maintained and instantaneous sources, source, Proc. Roy. Soc. Lond. Math. Phys. Sci. 234 (1956) 1–23. https://www.jstor.org/stable/99936.
[113] Y.J.P. Lin, T.H. Tsai, The push-type displacement ventilation in two series-connected chambers, Build. Environ. 62 (2013) 89–101, https://doi.org/10.1016/j.buildenv.2013.01.016.
[114] N.M. Mateus, G. Carrilho da Graça, A validated three-node model for displacement ventilation, Build. Environ. 84 (2015) 50–59, https://doi.org/10.1016/j.buildenv.2014.10.029.
[115] N.M. Mateus, G.N. Simões, C. Lúcio, G. Carrilho da Graça, Comparison of measured and simulated performance of natural displacement ventilation systems for classrooms, Energy Build. 133 (2016) 185–196, https://doi.org/10.1016/j.enbuild.2016.09.057.
[116] S. Nabi, P. Grover, C.P. Caulfield, Adjoint-based optimization of displacement ventilation flow, Build. Environ. 124 (2017) 342–356, https://doi.org/10.1016/j.buildenv.2017.07.030.
[117] S. Duan, C. Jing, E. Long, Transient flows in displacement ventilation enhanced by solar chimney and fan, Energy Build. 103 (2015) 124–130, https://doi.org/10.1016/j.enbuild.2015.06.006.
[118] X. Yang, Y. Kang, K. Zhong, Theoretical predictions of transient natural displacement ventilation, Build. Simulat. 6 (2013) 165–171, https://doi.org/10.1007/s12273-013-0098-7.
[119] A.B. Shrinivas, G.R. Hunt, Transient ventilation dynamics induced by heat sources of unequal strength, J. Fluid Mech. 738 (2014) 34–64, https://doi.org/10.1017/jfm.2013.579.
[120] X. Yuan, Q. Chen, L.R. Glicksman, Models for prediction of temperature difference and ventilation effectiveness with displacement ventilation, Build. Eng. 105 (1999).
[121] S. Zhang, Y. Cheng, C. Huan, Z. Lin, Modeling non-uniform thermal environment of stratum ventilation with supply and exit air conditions, Build. Environ. 144 (2018) 542–554, https://doi.org/10.1016/j.buildenv.2018.08.063.
[122] M. Camci, Y. Karakoyun, O. Acikgoz, A.S. Dalkilic, A comparative study on convective heat transfer in indoor applications, Energy Build. 242 (2021), https://doi.org/10.1016/j.enbuild.2021.110985.
[123] E. Mundt, Convection Flows above Common Heat Sources in Rooms with Displacement Ventilation, ROOMVENT '90, Oslo, Norway, June .
[124] Y. Li, M. Sandberg, L. Fuchs, Vertical temperature profiles in rooms ventilated by displacement: full-scale measurement and nodal modelling, Indoor Air 2 (1992) 225–249.
[125] E. Mundt, The Performance of Displacement Ventilation Systems Experimental and Theoretical Studies, Royal Institute of Technology, 1996 [Ph.D. Thesisi].
[126] Y. Li, Buoyancy-driven natural ventilation in a thermally stratified one-zone building, Build. Environ. 35 (2000) 207–214. www.elsevier.com/locate/buildenv.
[127] A.D. Arens, Evaluation of Displacement Ventilation for Use in High-Ceiling Facilities, Massachusetts Institute of Technology, 2000 [MSc Thesis].
[128] S.J. Rees, P. Haves, A nodal model for displacement ventilation and chilled ceiling systems in ooce spaces, Build. Environ. 36 (2001) 753–762. www.elsevier.com/locate/buildenv.
[129] X. Wu, B.W. Olesen, L. Fang, J. Zhao, A nodal model to predict vertical temperature distribution in a room with floor heating and displacement ventilation, Build. Environ. 59 (2013) 626–634, https://doi.org/10.1016/j.buildenv.2012.10.002.
[130] S. Zhang, Y. Cheng, C. Huan, Z. Lin, Heat removal efficiency based multi-node model for both stratum ventilation and displacement ventilation, Build. Environ. 143 (2018) 24–35, https://doi.org/10.1016/j.buildenv.2018.06.054.
[131] N. Lastovets, R. Kosonen, P. Mustakallio, J. Jokisalo, A. Li, Modelling of room air temperature profile with displacement ventilation, Int. J. Vent. 19 (2020) 112–126, https://doi.org/10.1080/14733315.2019.1579486.
[132] A. Novoselac, B.J. Burley, J. Srebric, Development of new and validation of existing convection correlations for rooms with displacement ventilation systems, Energy Build. 38 (2006) 163–173, https://doi.org/10.1016/j.enbuild.2005.04.005.
[133] H.B. Awbi, A. Hatton, Natural convection from heated room surfaces, Energy Build. 30 (1999) 233–244, https://doi.org/10.1016/S0378-7788(99)00004-3.
[134] N.M. Mateus, G. Carrilho da Graça, Simplified modeling of displacement ventilation systems with chilled ceilings, Energy Build. 108 (2015) 44–54, https://doi.org/10.1016/j.enbuild.2015.08.054.

[135] N. Lastovets, K. Sirén, R. Kosonen, J. Jokisalo, S. Kilpeläinen, Dynamic performance of displacement ventilation in a lecture hall, Int. J. Vent. 20 (2021) 204–214, https://doi.org/10.1080/14733315.2020.1777015.
[136] N. Lastovets, R. Kosonen, J. Jokisalo, The comparison of design airflow rates with dynamic and steady-state displacement models in varied dynamic conditions, Build. Simulat. 14 (2021) 1201–1219, https://doi.org/10.1007/s12273-020-0730-2.
[137] T. Yamanaka, H. Kotani, M. Xu, Zonal models to predict vertical contaminant distribution in room with displacement ventilation accounting for convection flows along walls, in: Roomvent – 10th International Conference on Air Distribution in Rooms, FINVAC, Helsinki, Finland, 2007. https://www.researchgate.net/publication/238715787.
[138] C. Habchi, K. Ghali, N. Ghaddar, Displacement ventilation zonal model for particle distribution resulting from high momentum respiratory activities, Build. Environ. 90 (2015) 1–14, https://doi.org/10.1016/j.buildenv.2015.03.007.
[139] Y. Cheng, B. Yang, Z. Lin, J. Yang, J. jia, Z. Du, Cooling load calculation methods in spaces with stratified air: a brief review and numerical investigation, Energy Build. 165 (2018) 47–55, https://doi.org/10.1016/j.enbuild.2018.01.043.
[140] W. Zhang, K. Hiyama, S. Kato, Y. Ishida, Building energy simulation considering spatial temperature distribution for nonuniform indoor environment, Build. Environ. 63 (2013) 89–96, https://doi.org/10.1016/j.buildenv.2013.02.007.
[141] C. Liang, X. Li, A.K. Melikov, X. Shao, B. Li, A quantitative relationship between heat gain and local cooling load in a general non-uniform indoor environment, Energy 182 (2019) 412–423, https://doi.org/10.1016/j.energy.2019.06.055.
[142] S. Zhang, Y. Cheng, C. Huan, Z. Lin, Equivalent room air temperature based cooling load estimation method for stratum ventilation and displacement ventilation, Build. Environ. 148 (2019) 67–81, https://doi.org/10.1016/j.buildenv.2018.10.057.
[143] S. Zhang, Z. Lin, P. Zhou, Y. Cheng, Fully mixed air model based cooling load estimation method for both stratum ventilation and displacement ventilation, Energy Build. 199 (2019) 247–263, https://doi.org/10.1016/j.enbuild.2019.07.005.